

THESIS

QUANTIFYING ASPECT-DEPENDENT SNOWPACK RESPONSE TO HIGH-ELEVATION  
WILDFIRE IN THE SOUTHERN ROCKY MOUNTAINS

Submitted by

Wyatt Reis

Department of Geosciences

In partial fulfillment of requirements

For the Degree of Master of Science

Colorado State University

Fort Collins, Colorado

Summer 2023

Master's Committee:

Advisor: Daniel McGrath

Stephanie Kampf

Michael Ronayne

Copyright by Wyatt Reis 2023

All Rights Reserved

## ABSTRACT

### QUANTIFYING ASPECT-DEPENDENT SNOWPACK RESPONSE TO HIGH-ELEVATION WILDFIRE IN THE SOUTHERN ROCKY MOUNTAINS

Seasonal snow is a critically important water resource for the western U.S., providing water for human consumption, hydropower, agricultural uses, and sustaining ecological biodiversity. However, due to a changing climate, seasonal snowpacks have declined by ~20% in the last century and the timing of annual runoff is occurring 1–3 weeks earlier than the historical normal. Wildfires are an additional disturbance that are impacting high-elevation seasonal snowpacks at significantly greater rates since 2000. The impacts of increased wildfire altered area introduces considerable water resources challenges due to the ways wildfire directly changes the mass and energy balances of seasonal snowpacks for years to decades following the disturbance. While the impacts of wildfire on seasonal snowpack are increasingly well documented, there is a lack of understanding in how impacts might vary across the complex terrain that characterizes these mountainous environments.

Utilizing burn-condition paired automated weather stations, regularly repeated burn-condition and aspect paired snow pits and snow depth transects, and snow depth measurements from time-lapse cameras within the 2020 Cameron Peak burn area during the second winter post-wildfire, I found no significant difference in peak snow water equivalent (SWE) between burned and unburned areas on both north and south aspects. Peak SWE was comparably greater (~100%) on north aspects in both burned and unburned areas. On burned south aspects, peak SWE occurred 22 days prior to burned north and all unburned areas. During the spring melt,

snow melted 147% faster on burned south aspects compared to unburned south aspects, while on burned north aspects, melt rates increased by ~60% relative to unburned slopes. The increase in melt rates on burned slopes was the result of energy balance differences, with the median daily net shortwave radiation increasing by 170%, while median daily longwave radiation fell by ~205%. However, the net energy evolved over the winter, with the sign of the daily net energy flipping in late March for both burned and unburned areas. In both instances, the magnitude of the net energy was greater in the burned area throughout the observed period. From late March through snow disappearance at the burned site, the net energy was ~60% greater at the burned site than the unburned weather station. My research provides a more nuanced understanding of wildfire impacts on seasonal snowpacks compared to previous work, as this work identified clear aspect-dependent differences in the response. These findings can be incorporated into physical models so water managers can better predict the timing and quantity of melt from these critical water resources in fire-impacted regions.

## ACKNOWLEDGEMENTS

I would like to thank my advisor, Dr. Dan McGrath, for taking me on as a student and providing consistent and continuous mentorship and direction throughout this project. Thank you to my committee members, Dr. Stephanie Kampf and Dr. Mike Ronayne, for their assistance and feedback in review of my work. To Dr. David Rey (USGS – Water Mission Area), thank you for your advisement and collaboration, I appreciate your patience and willingness to be a sounding board as I implemented my field plan and worked through my analysis. I am deeply humbled by the support Dr. Kelly Elder (USFS – Rocky Mountain Research Station) provided throughout my degree. Kelly has been extremely generous with his time and his guidance has shaped me as a scientist and person. I also thank Huihui Zhang and Kevin Yemoto with the USDA ARS in Fort Collins, CO for supporting the spectroradiometer observations.

I would also like to acknowledge, with respect, the significant amount of fieldwork that occurred on the traditional and ancestral lands of the Eastern Shoshone, Ute, Cheyenne, and Arapaho Nations and peoples. This fieldwork was made possible through the assistance of Amber Scott, John Kemper, Lucas Zeller, Megan Sears, Michael Reis, Anna Marshall, Aly Cheney, Payton Schiff, Nobu Endo, Dylan Weber, Eric McCue, and Holly Proulx.

I am in debt to the support and advisement I received from my friends and fellow students throughout the program. Thank you to Georgia, Mom, and Dad for always believing in me and for pushing me to be my best. Amber, thank you for your consistent support throughout my degree, your countless hours allowing me to talk at you about my research, editing my writing, and making sure I don't take myself too seriously have made my graduate school experience and final thesis significantly better. I am lucky to have you by my side through this crazy adventure.

This research was funded by The Geological Society of America Research Grant, the Colorado State University Evelyn I. Clark and Warner College of Natural Resources Scholarships, the Xi Sigma Research Grant, and the Colorado Mountain Club Foundation Research Grant.

## TABLE OF CONTENTS

ABSTRACT.....	ii
ACKNOWLEDGEMENTS.....	iv
LIST OF TABLES.....	viii
LIST OF FIGURES.....	ix
LIST OF EQUATIONS.....	x
1. Introduction.....	1
1.1 Western U.S. Seasonal Snow Climatology.....	1
1.2 Mass and Energy Balance of Seasonal Snowpacks.....	2
1.2.1 Seasonal Snow Accumulation in Complex Terrain.....	2
1.2.2 Terrain Controls of Energy Balance in Seasonal Snowpacks.....	3
1.2.3 Annual snow water equivalent estimation.....	5
1.3 Seasonal Snow in a Changing Climate.....	5
1.3.1 Forest Disturbances Altering Seasonal Snow Energy Balance.....	6
1.4 Increasing Wildfire Activity.....	8
1.5 Wildfire-Seasonal Snow Interactions.....	10
Study Objectives.....	13
2. Study Area.....	14
2.1 Site Description.....	14
2.2 Field Instrumentation.....	14
3. Methods.....	18
3.1 Field Methods.....	18
3.1.1 Automated Weather Stations.....	18
3.1.2 Manual Snowpack Measurements.....	19
3.1.3 Snow Surface Albedo Measurements.....	22
3.2 Data Processing.....	22
3.2.1 Snow Water Equivalent Calculations.....	22
3.2.2 Terrain Analysis and Cold Content.....	23
3.3 Snowpack Energy Balance.....	24
3.3.1 Shortwave and Longwave Components.....	24
3.3.2 Turbulent Energy Flux Modeling.....	25
4. Results.....	28
4.1 Influence of Complex Terrain.....	28
4.1.1 Quantity and Timing of Peak SWE.....	28
4.1.2 Melt Rates and Timing.....	31
4.2 Snowpack Preconditioning Following Wildfire.....	32
4.3 Wind Speed Following Wildfire.....	33
4.4 Energy Balance Following Wildfire.....	34
4.4.1 Shortwave Radiation Balance.....	34
4.4.2 Longwave Radiation Balance.....	38
4.4.3 Net Radiation Balance.....	39
4.4.4 Turbulent Heat Fluxes.....	39
4.4.5 Net Energy.....	40

5. Discussion .....	44
5.1 Snowpack Accumulation and Melt .....	44
5.1.1 Peak SWE Timing and Quantity .....	44
5.1.2 Aspect Influence .....	45
5.2 Snowpack Energy Balance .....	46
5.2.1 Snowpack Albedo .....	49
5.3 Additional Considerations .....	52
5.3.1 Influence of Albedo and Pre-wildfire Tree Mortality .....	52
5.3.2 Influence of Snow Zone .....	53
5.3.3 Influence of Snow Regime .....	55
6. Future Work .....	57
7. Conclusions .....	60
REFERENCES .....	62

## LIST OF TABLES

Table 1. Study Site Locations and Characteristics.....	17
Table 2. Fieldwork Dates and Observation Summary .....	21

## LIST OF FIGURES

Figure 1. Representative Peak SWE for Mountainous Regions of North America.....	2
Figure 2. Western US Wildfire Burned Area Trends (1984–2020).....	9
Figure 3. Typical Seasonal Snowpack Changes Following Wildfire .....	11
Figure 4. Cameron Peak Wildfire Study Area Map.....	16
Figure 5. Time-lapse Camera Site Photos.....	19
Figure 6. Aspect and Burn Condition-based Snowpack Timeseries.....	30
Figure 7. Daily Spring SWE Change .....	32
Figure 8. Snowpack Cold Content .....	33
Figure 9. Post-Wildfire Wind Speed.....	34
Figure 10. Snowpack Spectral and Broadband Albedo .....	38
Figure 11. Boxplots of Daily Shortwave, Longwave, and Net Radiation Fluxes.....	36
Figure 12. Daily Net Radiation, Turbulent Fluxes, and Net Energy Balance .....	43
Figure 13. Late Fall Near-IR Satellite Imagery of the Study Area.....	46
Figure 14. Post-Wildfire Aspect-based Mass and Energy Balance Schematic .....	49
Figure 15. Late-Season Snow Accumulation by Snow Zone .....	51
Figure 16. Black Carbon on Trees in the Study Area.....	53

## LIST OF EQUATIONS

(1).....	23
(2).....	23
(3).....	24
(4).....	24
(5).....	24
(6).....	25
(7).....	25
(8).....	25
(9).....	25
(10).....	26
(11).....	26
(12).....	26
(13).....	26
(14).....	27
(15).....	27

# 1. INTRODUCTION

## 1.1 Western U.S. Seasonal Snow Climatology

Seasonal snowpacks are critical to regulating the global surface energy balance and hydrologic cycle due to snow's high albedo and the seasonal storage and delivery of water (Barnett et al., 2005; Groisman et al., 1994; Namias, 1985). At its maximum extent, seasonal snow covers up to ~60% of the total land area in the Northern Hemisphere (Hammond et al., 2018; Moore et al., 2015). The large spatial extent, combined with a high albedo (~0.8), reduce the radiative forcing at a regional scale, and controls carbon exchange to the atmosphere (Zhang, 2005). While the seasonal snow cover is widely distributed in the Northern Hemisphere, up to 60% of seasonal snow mass accumulates in mountains across the region (Figure 1; Wrzesien et al., 2018). The water stored in these high-elevation snowpacks, or snow water equivalent (SWE), is critically important to downstream ecological health, human consumption, and economies based on outdoor recreation and agriculture (Barnett et al., 2005; Sturm et al., 2017). The slow release of water during annual melt is pivotal in promoting ecosystem biodiversity, maintaining soil moisture, and initiating seasonal plant growth for headwater areas and downstream lowlands (Blankinship et al., 2014; Corriveau et al., 2011; Keller et al., 2005).

In the western U.S., most watersheds have distinct seasonal cycles that are dominated by the accumulation of seasonal snowpacks from late fall to early spring, followed by the slow release of water, which supplies 60–80% of streamflow during the spring and summer when water demands are greatest (Bales et al., 2006; Barnett et al., 2005; D. Li et al., 2017; Sturm et al., 2017; Viviroli et al., 2007). The Colorado River Basin is a prominent example of a snow-dominated watershed in the region—it alone provides water to 40 million people and 5.5 million

acres of crop lands (*Colorado River Basin Water Supply and Demand Study Executive Summary*, 2012).

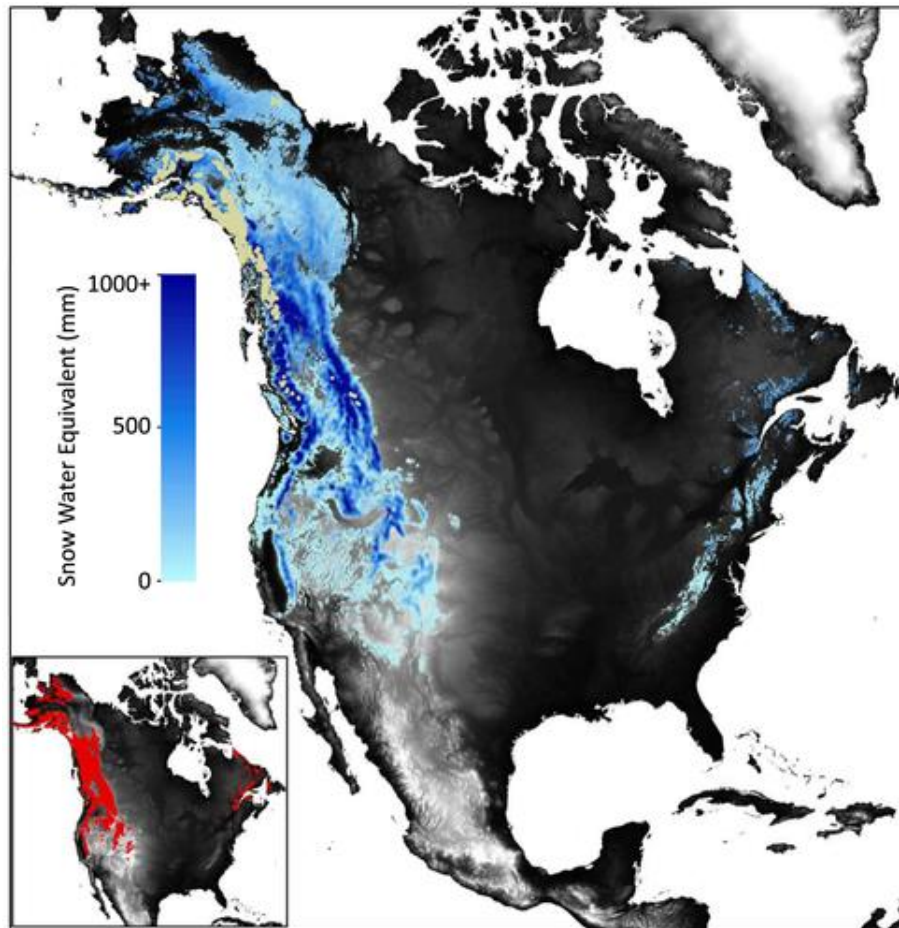


Figure 1. Representative peak snow water equivalent (SWE) for mountainous regions of North America from Weather Research and Forecasting (WRF) simulations for each mountain range. Tan areas are glaciers and not represented. Inset shows the 30% of grid cells which make up 75% of the total SWE in all mountainous areas. Figure from Wrzesien et al. (2018).

## 1.2 Mass and Energy Balance of Seasonal Snowpacks

### 1.2.1 Seasonal Snow Accumulation in Complex Terrain

Despite the demonstrated importance of snowmelt, it remains difficult to accurately measure or model the volume of water stored in mountainous watersheds each year. This difficulty in measuring the amount of snow within a mountainous watershed is due to the high

spatiotemporal variability of snow in these environments (Anderton et al., 2004; Bonnell et al., 2021; Elder et al., 1991, 1998; Miller et al., 2022; Trujillo et al., 2009) and limitations in existing measurement locations (e.g., SNOTEL) and satellite-based methodologies. The current technology for real-time in-situ measurement locations that may exist in a watershed are typically optimized for measurement below the alpine regions and may not fully capture the SWE within a watershed, particularly late in the melt season (Molotch & Bales, 2006; Schneider & Molotch, 2016; Serreze et al., 1999). Snow depths and SWE is highly variable at the plot, watershed, and regional scales due to complex interactions between vegetation and topographic features which alter wind speed, precipitation, and energy fluxes (Elder et al., 1989; Liston et al., 2007; López-Moreno et al., 2011; Trujillo et al., 2007, 2009). Snow accumulation is highly dependent on canopy interception (Pomeroy et al., 1998; Storck et al., 2002; Winkler et al., 2005). In vegetated areas, canopy interception of snowfall reduces the snow accumulation on the ground surface by up to 60% of total snow fall and sublimation losses of snow from conifer canopies can reach 30% of total snowfall (Hedstrom & Pomeroy, 1998; Molotch et al., 2007; Montesi et al., 2004; Sexstone et al., 2018). In topographically complex locations, snow accumulation is driven by orographic depositional patterns on windward alpine slopes, however these slopes are typically exposed to increased wind speeds, causing scour on windward slopes and increased deposition on leeward aspects (Mott et al., 2014).

### **1.2.2 Terrain Controls of Energy Balance in Seasonal Snowpacks**

Seasonal snowpack energy balances are primarily controlled by shortwave, longwave, and turbulent energy fluxes, with the magnitude of each component varying with ecoregion, seasonality, and topographic and vegetative controls (Dozier et al., 2016a; Elder et al., 1991). The primary source of energy input is shortwave radiation from the sun, with the amount of

energy absorbed by the snowpack modulated by the surface albedo, or ratio of outgoing and incoming shortwave radiation. In the mid-latitudes, snowpack ablation rates are highly dependent on the quantity of absorbed shortwave radiation (Marks et al., 1992; Marks & Dozier, 1992; Painter, Molotch, et al., 2007). The Earth's surface and atmosphere emit longwave radiation which then interacts with the seasonal snowpack through the transfer of heat. For example, in forested areas, trees emit longwave radiation and in turn warm the snowpack. Longwave energy can drive negative net surface energy balances, particularly in the early to mid-winter period when available shortwave radiation is low, leading to an energy deficit and cold content development. The longwave budget can also initiate and drive snow melt at high-latitude or cloudy sites where solar radiation zenith angles are low (Sicart et al., 2006). Turbulent fluxes, sensible and latent heat, are typically lower magnitude components of the energy balance. However, they are important to understand due to the differences between open and forested areas. Turbulent fluxes drive snow mass loss via sublimation, with open areas experiencing greater magnitudes of turbulent flux energy and mass loss than forested locations (Boon, 2009).

Within the complex terrain that often characterizes mountainous environments, modelling the amount of solar radiation can be difficult due to the intricate relationships between direct and indirect incoming solar radiation which are a function of the local aspect, canopy, and the surrounding topography available for shading (Lee et al., 2011; Picard et al., 2020; Sirguey et al., 2009). The inability to accurately model these relationships has been found to introduce up to 10% error in surface energy balance models (Lee et al., 2011). Within persistent snow zones (Sturm et al., 1995; Sturm & Liston, 2021), these large gradients in available shortwave radiation force significant differences in peak SWE and SWE melt rates, resulting in decreased SWE and

higher melt rates on south and west aspects (Anderson et al., 2014; Dozier, 1980; Duguay, 1993; Elder et al., 1991; Williams et al., 1972).

### **1.2.3 Annual snow water equivalent estimation**

Currently, water managers and the scientific community use empirical and physical models to predict the quantity of water stored in the seasonal snowpack and the timing of melt each year. However, these models rely on historic norms which are increasingly unrepresentative of modern snow accumulation, rain-snow fractions, and melt rates (Hammond & Kampf, 2020; Klos et al., 2014; Mote, 2006; Siirila-Woodburn et al., 2021), severely hampering the ability for accurate forecasting (Meyer et al., 2023a). Due to the limitations of in-situ measurements in these highly complex systems, considerable effort is being devoted to assimilating remote sensing observations into modelling frameworks to build tools for real-time operational water resource measurement (Dozier et al., 2016b; H. P. Marshall et al., 2019).

## **1.3 Seasonal Snow in a Changing Climate**

The divergence from historic norms is driven by anthropogenic climate change, with a ~20% decrease of 1 April snowpack since 1915 across the western U.S. (Mote et al., 2005, 2018). Climate change is not only decreasing the quantity of snow but is also impacting the timing and rate of melt. Melt timing in Colorado shifted 1–3 weeks earlier between 1978–2008 (Clow, 2010; Dudley et al., 2017), a finding that is consistent in the western U.S. (Cayan et al., 2001; Hall et al., 2015; McCabe & Clark, 2005; Wagner et al., 2021). Since snowpacks are melting earlier in the season, less solar radiation is available due to low solar zenith angles and shorter duration days, which causes reduced melt rates and may subsequently lead to increased

evapotranspiration and less runoff generation (Barnhart et al., 2016; Musselman et al., 2017). Between 1984–2017, snowmelt rates decreased by as much as 20% and melt initiated 8 days earlier per decade in the Rio Grande headwaters in southern Colorado (Sexstone et al., 2020). Across the western U.S., climate change is further increasing seasonal snowpack interannual, temporal, and spatial variability (Dye, 2002), shown by elevation and ecoregion dependence in changes in peak SWE, and timing and rate of melt (Hammond et al., 2023; A. M. Marshall et al., 2019; Smoot & Gleason, 2021). Given future climate projections, the hydrology within snow-dominated watersheds is expected to bifurcate based on elevation with the lowest elevations moving toward dramatically declined peak SWE (14–45%), while peak SWE at high elevations remains nearly unchanged, but melt is projected to begin ~3 weeks earlier at all elevations (Hammond et al., 2023). This increased variability in snowpack accumulation and melt leads to “flashier” systems (decreased hydrograph duration) due to more liquid precipitation and earlier timing, resulting in projected greater unpredictability of drought conditions in 69–83% of snowmelt-dominated areas by the end of the century (Hammond et al., 2023; Livneh & Badger, 2020). Additionally, the changing timing and phase of winter precipitation and earlier snowmelt/spring runoff within these snow-dominated watersheds reduces water storage and increases aridity, increasing the potential for wildfire activity and burned area during subsequent summers with the earliest third of snow disappearance dates leading to 70% of the area burned by large wildfires from 1970–2012 (O’Leary et al., 2016; Westerling, 2016).

### **1.3.1 Forest Disturbances Altering Seasonal Snow Energy Balance**

In the western U.S., most of the snow accumulates in in high-elevation evergreen and deciduous forests, primarily composed of Douglas-fir (*Pseudotsuga menziesii*), Subalpine fir

(*Abies lasiocarpa*), Engelman Spruce (*Picea engelmannii*), Lodgepole pine (*Pinus contorta*), Ponderosa pine (*Pinus ponderosa*), and Quaking aspen (*Populus tremuloides*; Mathys et al., 2017; Stanke et al., 2021). The high-elevation forests in turn exert strong control on the accumulation and melt rates of the snowpack (Biederman et al., 2014; Musselman et al., 2008; Roth & Nolin, 2017; Troendle & King, 1985). For example, in northern New Mexico, canopy interception reduced peak SWE by 47% and melt rates by 54% (Musselman et al., 2008). However, these forests are constantly evolving and significant human and climate induced catalysts including silviculture, insect infestations, and wildfire have caused dramatic changes to the high-elevation forests of the western U.S. in recent decades (Biederman et al., 2014; Kampf et al., 2022; Seidl et al., 2017). Changes to the forest structure then modulate the mass and energy balances of the seasonal snowpack, altering the processes which dictate seasonal accumulation and melt processes, and expanding the variability and uncertainty in understanding snowpack physical processes and hydrologic outputs (Biederman et al., 2014; Granger & Pomeroy, 1997; C. D. Murray & Buttle, 2003; Troendle & King, 1985).

Given the value of snow and the pronounced changes that are occurring, there is an increased interest in how snowpack processes are altered due to changing energy balances from increased insect infestation, rain-on-snow events, dust-on-snow events, and wildfire (Boon, 2009, 2012; Burles & Boon, 2011; Clow et al., 2016; McCabe et al., 2007). For example, from 1993–2014 there was an 81% increase in winter and spring dust deposition in the southern Rockies (Clow et al., 2016), while from 1949–2013 there were significant increases in the number of rain-on-snow events at high elevations of the western U.S. (Cohen et al., 2015; McCabe et al., 2007). The impacts of these forest disturbances and changes in energy inputs is a fundamental alteration of the snowpack energy balance, driving earlier and/or rapid snowmelt.

Following a wildfire or insect infestation (e.g., beetle kill), the reduction in forest canopy increases the amount of energy incident on the snowpack surface, resulting in a more positive energy balance and increased melt rates (Boon, 2009; Burles & Boon, 2011). The increased deposition of dust or black carbon (e.g., wildfire soot) on seasonal snowpacks decreases the surface albedo of the snowpack and directly increases the radiative transfer of shortwave energy into the snowpack, accelerating snowmelt (Clow et al., 2016; Gleason et al., 2013; J. Li et al., 2013; Skiles et al., 2018). Rain-on-snow events alter the snow energy balance through the direct energy input caused by the increased energy held by the liquid precipitation, a process that can initiate to rapid melt rates and flooding (Cohen et al., 2015; McCabe et al., 2007).

#### **1.4 Increasing Wildfire Activity**

Beginning in the mid-1980s, wildfire burn area, severity, and mean elevation increased rapidly across the western U.S. (Alizadeh et al., 2021; Westerling et al., 2006), and in the early 2000s there was an additional pronounced increase in wildfire frequency and size (Iglesias et al., 2022; Shi & Touge, 2023). Both increases in wildfire activity were driven by anthropogenic climate change, availability of fuels due to a history of fire suppression, and increased human activity in remote areas (Abatzoglou & Williams, 2016). Between 1984–2017 western U.S. forests above 2500 m experienced a 270% increase in wildfire activity, with the median burned elevation increasing by 250 m (Alizadeh et al., 2021). In the Idaho Batholith, 50% of forested area has burned since 1984 (Kampf et al., 2022). Future climate predictions and availability of fuels indicate that these trends will continue to occur for decades to come (Mueller et al., 2020; Westerling et al., 2011), with both static and dynamic models of wildfire-fuel availability

indicating 63–107% increases in projected mean annual burn area by the end of the century (Abatzoglou et al., 2021).

Due to the expansion of fire to these high-elevation forests, seasonal snow zones have been increasingly impacted by wildfire. Since 1984, there has been a significant increase in burned area within the late season snow zone in 70% of western U.S. ecoregions, and the Southern Rockies have seen a significant increase in proportion of burned area in the late and middle season snow zones (Figure 2; Kampf et al., 2022). These increases in wildfire within headwater seasonal snow zones and the impacts of wildfire on snowpacks greatly alter the hydrologic responses in these watersheds. Most burned areas have experienced both an increase in peak SWE and spring melt rates (Giovando & Niemann, 2022; Loiselle et al., 2020; Maina & Siirila-Woodburn, 2020; Smoot & Gleason, 2021), which adds to the considerable operational challenge already facing water resources in the western U.S.

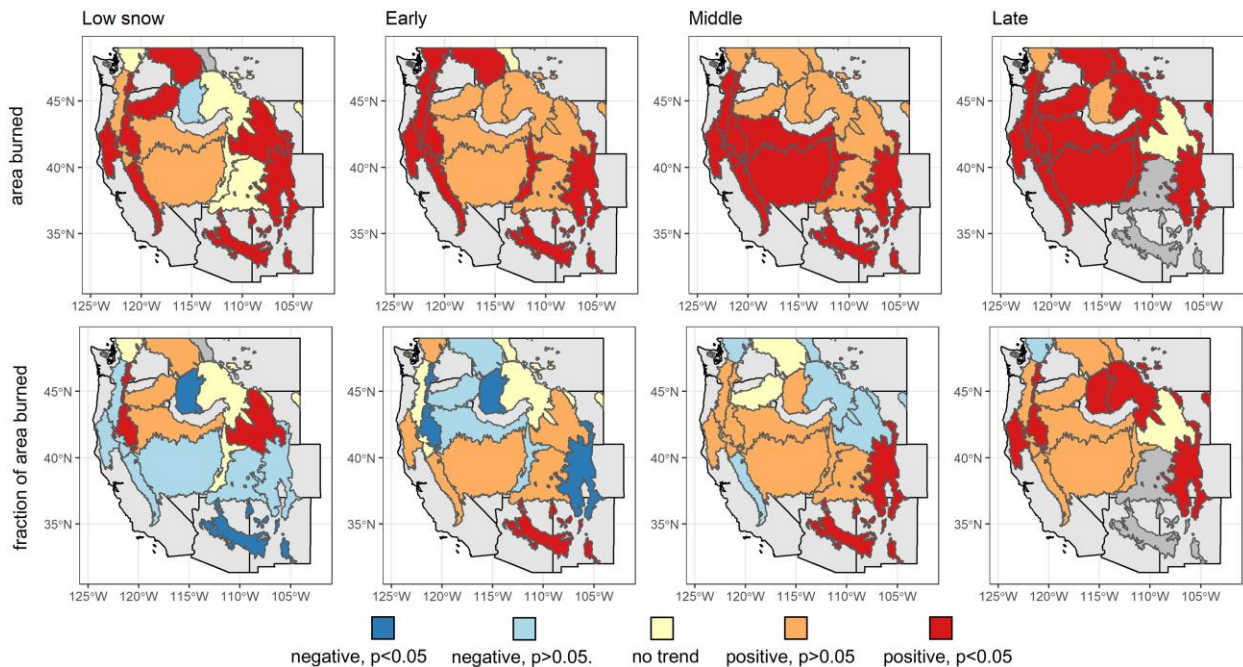


Figure 2. Burned area trends by EPA Level III Ecoregions and snow persistence zone for the western U.S. between 1984 and 2020 using the Mann-Kendall test. Figure from Kampf et al. (2022).

## 1.5 Wildfire-Seasonal Snow Interactions

Wildfire directly alters the forest structure by reducing or completely removing the canopy which is essential to regulating the mass and energy balance of seasonal snowpacks. By removing this canopy, the accumulation and melt patterns of seasonal snowpacks are altered due to pronounced changes to the mass and energy balances. This occurs in four primary ways: (i) a reduction in canopy interception due to canopy loss (Harpold et al., 2014; McGrath et al., 2023) and (ii) an increase in shortwave radiation reaching the snow surface (Burles & Boon, 2011), (iii) a lower snow surface albedo from soot/burned debris on the surface (Gleason et al., 2013; Gleason & Nolin, 2016; Uecker et al., 2020), and (iv) increases in turbulent fluxes because of higher wind speeds at the snow surface (Boon, 2009; Molotch et al., 2009). These energy balance alterations are present in all post-fire environments, typically resulting in greater accumulation, increased snowmelt rates, and earlier snow disappearance, however the quantity of peak SWE varies by ecoregions (Figure 3; Giovando & Niemann, 2022; Koshkin et al., 2022; Smoot & Gleason, 2021).

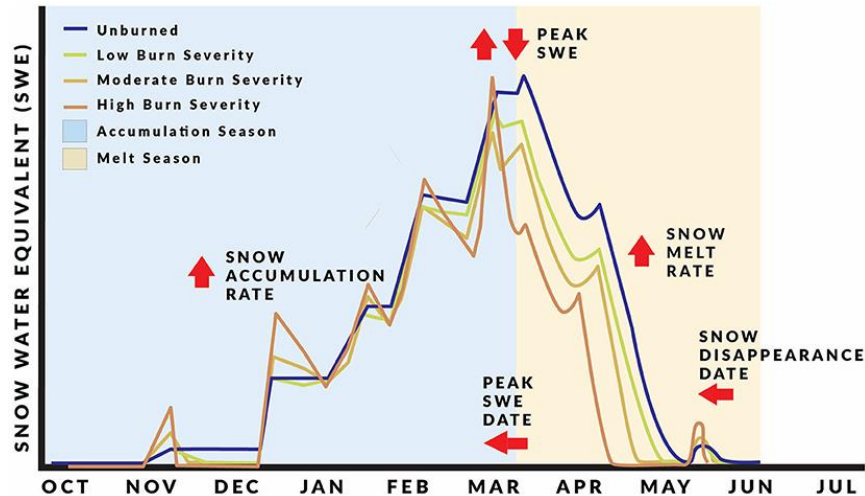


Figure 3. Typical western U.S. snowpack changes following wildfire based on burn severity with arrows indicating the relative shift of each of snowpack mass balance indicators. Figure from Koshkin et al. (2022).

Using paired SNOTEL stations across the western U.S., both Giovando & Niemann (2022) and Smoot & Gleason (2021) found reductions in peak SWE following disturbance at the 60% of sites. For some regions, notably the Northern Rockies and Arizona-New Mexico Mountains, peak SWE increased by 7%. These results confirm the dichotomy present in existing post-wildfire snowpack literature where plot to fire-scale studies have documented differences in the snowpack response during the accumulation period. Previous studies have consistently found greater melt rates during the spring in fire-impacted areas, with a combination of low snow surface albedo and increased solar radiation reaching the surface driving an increase in the radiative forcing (Burlles & Boon, 2011; Gleason et al., 2013; Harpold et al., 2014). The duration of snowpack process recovery following wildfire is unknown, in large part because the trajectory depends on the pace of vegetation recovery. At a minimum, previous work has shown that the snow surface albedo recovery can persist for more than decade following a wildfire (Gleason et al., 2019). More concerning though is the current trend of trees struggling to germinate post-

wildfire, causing the landscape to transition to grasslands (Rodman, Veblen, Battaglia, et al., 2020; Rodman, Veblen, Chapman, et al., 2020; Rother & Veblen, 2016; Stevens-Rumann et al., 2018). Due to the lack of canopy regeneration, the post-wildfire increase of incoming shortwave radiation will permanently alter the snowpack energy balance. Wildfire burn severity is a key control over the snowpack energy balance recover rate, with low severity fires recovering quicker than areas more severely impacted by the wildfire (Koshkin et al., 2022; Uecker et al., 2020). However, this is worrisome, as wildfire burn severity has increased significantly over much of the western U.S. during recent decades (Dennison et al., 2014).

While the importance of aspect for seasonal snowpack energy balances is well understood, most previous wildfire-snowpack interaction studies have not focused on identifying the ways post-fire snowpack processes are modulated by complex terrain. In the studies that incorporate differences in aspect, wildfire influenced snow depth with the greatest decreases occurring on south aspect slopes (Maxwell et al., 2019; Moeser et al., 2020). The key knowledge gap surrounding the influence of complex terrain on wildfire-alter seasonal snowpacks motivates this current study.

## STUDY OBJECTIVES

I address the knowledge gap in aspect-related differences using paired automated weather station data and field snowpack measurements across aspect and burn conditions. My three central research questions were: i) how does wildfire alter the quantity and date of peak SWE across complex terrain?, ii) how does complex terrain alter the ablation patterns within the burned zone?, and iii) how do different components of the seasonal snowpack energy balance compare between burned and unburned areas with similar terrain complexity?

To answer these questions, I collected multiple sources of data continuously or every other week from late November until mid-June. Continuously, I collected hourly automated weather station data at two paired burned/unburned sites and hourly snow depth using time-lapse cameras and snow poles at three additional locations. I chose the automated weather station and time-lapse camera locations based on the aspect and burn condition in order to capture areas untouched or severely burned by the fire on north and south topographic aspects. Every other week I collected snow pit data at each of the five automated weather station or time-lapse camera sites. Additionally, every other week I collected snow depth along four transects which captured a variety of north and south aspects within burned and unburned areas.

I then used these datasets to determine: i) peak SWE magnitudes, ii) peak SWE dates, iii) melt rates, and iv) energy balance. By combining observations that spanned different aspects, as well as burned and unburned locations, I was able to directly compare the SWE magnitudes, dates, and melt rates across all conditions. While the net radiometers on the paired burned and unburned automated weather stations allowed for direct comparison of the energy balance under each burn condition.

## 2. STUDY AREA

### 2.1 Site Description

I established a study area at an elevation of ~3050 m within the sub-alpine zone of the Cache la Poudre watershed approximately 5 km east of the Cameron Pass summit in northcentral Colorado (Figure 4a, Figure 4b, and Figure 4c). The 2 km<sup>2</sup> study area is situated in a mixed forest of Subalpine fir (*Abies lasiocarpa*), Douglas fir (*Pseudotsuga menziesii*), and Engelmann spruce (*Picea kampf engelmannii*). The 2020 Cameron Peak wildfire which was ignited on 13 August and burned 845 km<sup>2</sup> of the Cache la Poudre and lower Big Thompson watersheds burned portions of the study area (*Cameron Peak Fire BAER*, 2020). The study area sampled the range of burn severities present within the burned persistent seasonal snow zone (SSZ; Figure 4f; Moore et al., 2015), but given specific conditions in the study area, oversampled high burn severities and under sampled low to moderate burn severities (Figure 4f). Additionally, while the study site spanned the range of northness values within the burned SSZ, there was a slight negative skew, indicating somewhat more north-facing slopes (Figure 4g).

### 2.2 Field Instrumentation

Within the study area, I chose six study sites across a variety of aspects and burn conditions (Table 1), and installed a second automated weather station (AWS) in a ~5 by 5 m forest opening representative of unburned forest in the area (Unburned – AWS) to complement the AWS previously installed in a high burn severity location (Burned – AWS; Figure 4). Additionally, I used an automated sonic depth sensor that was previously installed in an unburned under canopy location (Unburned – UC). All three of these automated sites have a similar southeast aspect (–0.12–0.02) and are on relatively flat terrain (2.8–6.3°; Table 1). I

established the three additional sites on sloped terrain (Burned – North, Burned – South, Unburned – North; Table 1; Figure 4b and Figure 4c). At both meteorological sites and at the three additional sloped sites I hung time-lapse cameras along with snow poles. I visited these five sites (two AWS and three sloped) every other week from mid-November through mid-June to excavate and sample snow pits. In addition to these point measurements, I conducted four ~500 m snow depth transects every other week. The snow depth transects covered a range of terrain aspects and burn conditions (Figure 4b and Figure 4c).

In addition to the six sites established within the primary study area, I also used data from the Joe Wright SNOTEL (ID 551) to characterize an unburned open site (i.e., with limited canopy interception) and understand the context of seasonal SWE totals. The Joe Wright SNOTEL is located about 80 m higher and 3.5 km southwest of the main study area (Table 1). In 2021–2022, SWE at the Joe Wright SNOTEL was close to average, with a maximum SWE of 632 mm on 10 May compared to the 1991–2020 median of 622 mm on 6 May. Snow disappearance occurred on 15 June, two days earlier than the 17 June median snow disappearance date (SDD).

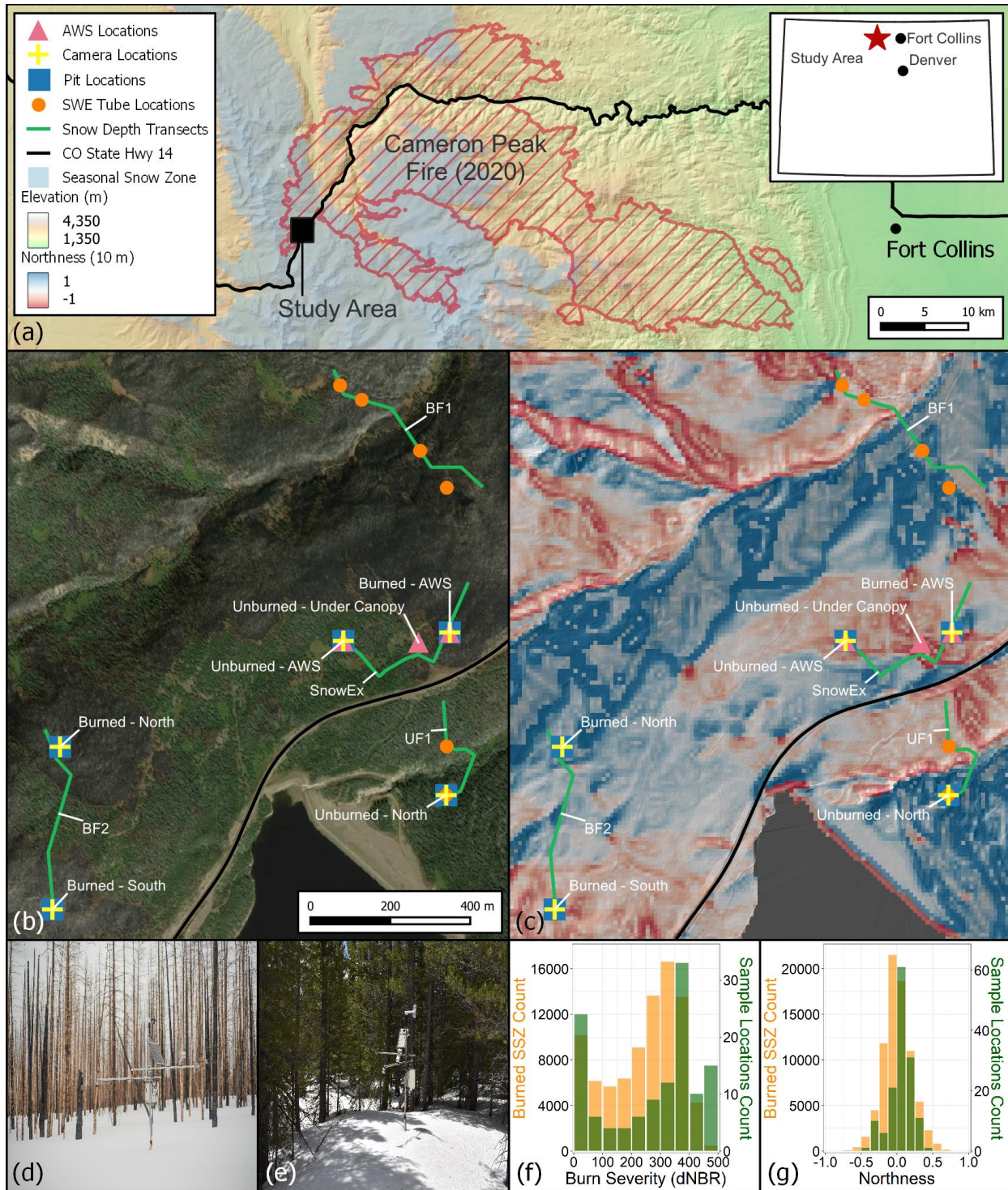


Figure 4. Study area location with respect to the 2020 Cameron Peak wildfire burn area and the persistent seasonal snow zone (SSZ; Moore et al., 2015) (a). Maxar optical imagery of the study area from the summer following the fire to show burn severity and study site locations (b). The 10 m average northness is show for the study area (c). Northness was derived from the 2021 post-fire lidar (0.67 m DEM) and down sampled to 10 m resolution for viewing clarity. A

photograph of the burned AWS which was installed in January 2021 (d). A photograph of the unburned AWS which was installed in November 2021 in a ~5 m by 10 m forest opening (e). Histogram of binned differenced normalized burn ratio (dNBR) within the SSZ impacted by the Cameron Peak fire (orange) and at each of the repeat snow depth transect locations (green) (f). Histogram of northness values (0.67 m resolution) within the burned SSZ (orange) and the sampled locations (green) (g).

Table 1. Study site locations, difference normalized burn ratios (dNBR), elevations, and topographic characteristics.

<b>Site Name</b>	<b>Coordinates (degrees)</b>	<b>dNBR (unitless)</b>	<b>Elevation (m)</b>	<b>Aspect (deg)</b>	<b>Slope (deg)</b>	<b>Northness (-1 to 1)</b>
Burned – AWS	(40.564, – 105.867)	373	3009	64.7	2.3	0.02
Burned – North (Camera)	(40.561, – 105.879)	355	3095	41.3	12.6	0.16
Burned – South (Camera)	(40.558, – 105.879)	464	3102	220.6	19.8	–0.26
Unburned – AWS	(40.563, – 105.870)	-	3019	176.2	6.8	–0.12
Unburned – North (Camera)	(40.560, – 105.867)	-	2991	15.5	23.9	0.39
Unburned – Under-Canopy (UC)	(40.564, – 105.868)	-	3010	169.4	4.6	–0.08

## 3. METHODS

### 3.1 Field Methods

#### 3.1.1 Automated Weather Stations

The burned automated weather station (AWS) was installed in January 2021, and the unburned AWS was installed in November 2021. Both weather stations measure air temperature and relative humidity (*Campbell Scientific HydroVUE5*), snow depth (*Campbell Scientific SR50A*), snow/soil temperature and relative permittivity (*Campbell Scientific SoilVUE10*; *unburned, 1 m; burned, 0.5 m*), wind speed and direction (*RM Young 05103 Wind Monitor*), barometric pressure (*Campbell Scientific CS100; burned only*) and the four-component net radiation balance (*Apogee SN500SS*). The AWS sites were programmed to collect data every minute and logged the fifteen minute and hourly mean values. The Unburned–Under Canopy (UC) site was also instrumented in January 2021 with an A2 Photonic Sensors SPICE standalone sonic depth sensor (Figure 4b and Figure 5f).

I also measured snow depth at the two AWS sites and at three additional snow depth sites using time-lapse cameras and snow poles with 10 cm gradation (Figure 4b and Figure 5). At the time-lapse sites, I installed three snow depth poles at locations without a weather station or one pole at the AWS sites crossover sites. I programmed the time-lapse cameras to capture a photo hourly between 0700 and 1900. I then manually recorded daily snow depths with 5 cm precision from the noon (1200) or next interpretable photo.

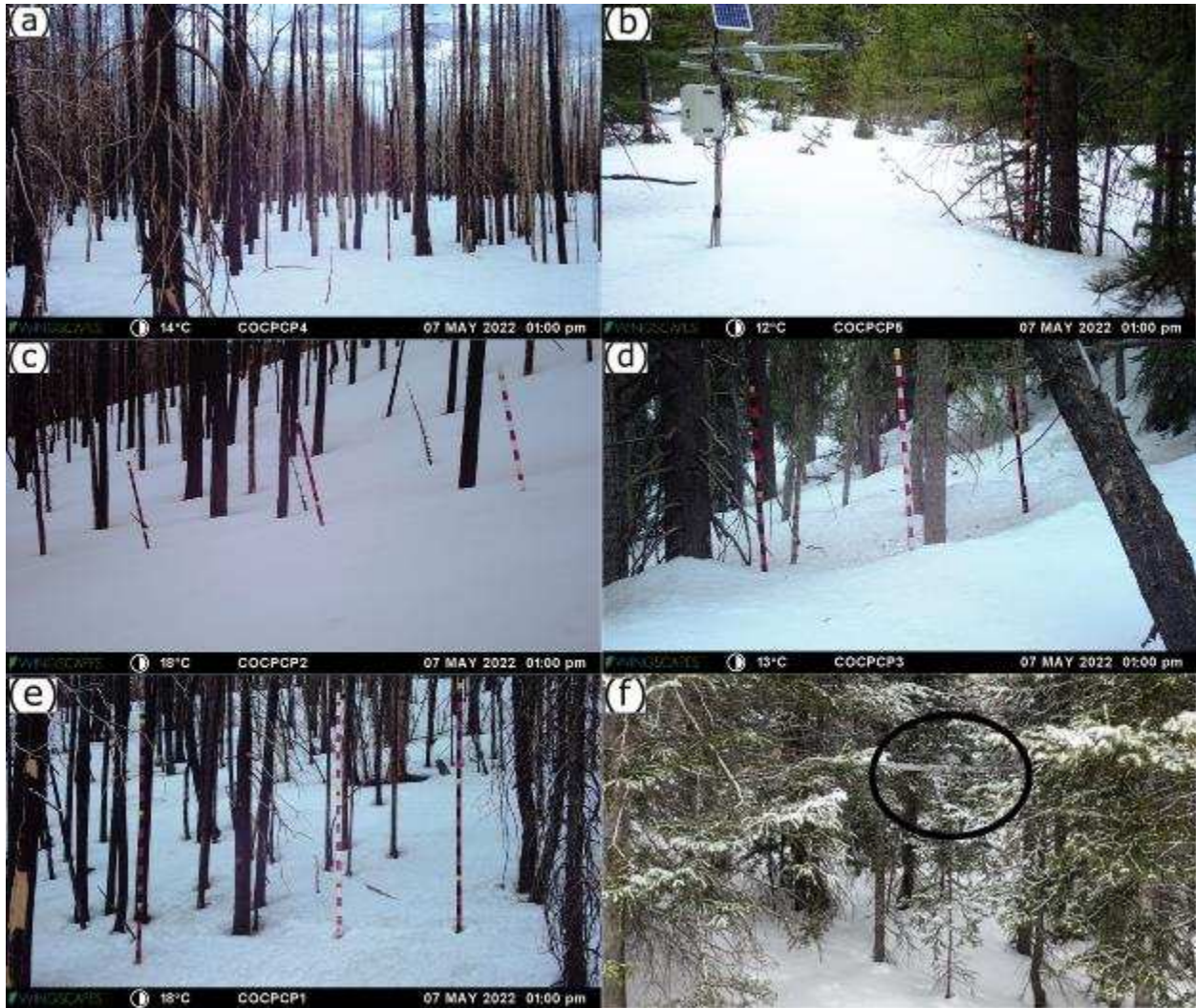


Figure 5. Time-lapse camera photos of the snow poles from 7 May at 1300 the (a) burned AWS, (b) unburned AWS, (c) burned north, (d) unburned north, and (e) burned south. Also shown is the unburned under-canopy site with the A2 Photonic Sensors SPICE unit circled (f).

### 3.1.2 Manual Snowpack Measurements

From 14 November – 13 June, I collected snow pit and snow depth transect data approximately every other week (Table 2). Snow pits were co-located with the two AWS and three snow depth sites. Snow pit observation profiles included snow density, dielectric permittivity, temperature, snow stratigraphy, and grain size. The snow pits were in the same general location each time but were shifted ~1 m behind the previous pit to minimize the

influence of the previous pit face. Pits were dug with the measurement wall facing north and were backfilled following data collection.

I collected snow depths along four transects during the same week as we conducted the snow pit observations (Table 2). I used a 3 m Snowmetrics probe with 1 cm gradations to collect snow depth in a 1 m five-point “star” pattern (Harpold et al., 2014), every ~15 m along the four ~500 m transects. Each snow depth was geolocated using a Juniper Systems Geode GNSS receiver (<30 cm horizontal accuracy) mounted on the top of the snow probe, allowing us to collect snow depth in repeat locations throughout the winter. I then calculated the mean snow depth for each “star” location using the five depth samples. I then assigned the slope, aspect, and burn condition to each “star” location based on the post-fire 2021 lidar-derived DEM (0.7 m resolution) and the post-fire difference Normalized Burn Ratio (dNBR) burn severity map (Woodward and Vorster, unpublished). The dNBR map was calculated following the wildfire by subtracting a post-fire Normalized Burn Ratio (NBR) from a pre-fire NBR, which are a ratio of the near-infrared (NIR; 0.76–0.90  $\mu\text{m}$ ) and shortwave infrared (SWIR; 2.08–2.35  $\mu\text{m}$ ) values from satellite and aerial imagery. This method is the standard for examining the burn severity of wildfire-impacted areas since the combination of NIR and SWIR distinctly highlight areas that have burned and the change in the values following the fire is used to show the severity of that burn. While completing the transects, we collected additional bulk snowpack density measurements using a Snow-Hydro SWE Coring Tube at six locations (Figure 4b).

Table 2. Dates of fieldwork during the 2021–22 winter and the snow pit or transect data collected on each date. Dates SfM were flown are also included. Due to time constraints, BF1 was collected on 19 November instead of 14 November.

<b>Snow Pit Dates</b>	<b>Pit Profiles Collected</b>	<b>Depth Transect Dates</b>	<b>Transects Completed</b>
14-Nov	Density, Temperature, Stratigraphy	14-Nov; 19-Nov	BF2, UF1, SNOWEX; BF1
28-Nov	Density, Temperature, Stratigraphy	28-Nov	BF1, BF2, UF1, SNOWEX
13-Dec	Density, Temperature, Stratigraphy	17-Dec	BF1, BF2, UF1, SNOWEX
27-Dec	Density, Temperature, Stratigraphy	28-Dec	BF2, SNOWEX
10-Jan	Density, Temperature, Stratigraphy	12-Jan	BF1, BF2, UF1, SNOWEX
24-Jan	Density, Temperature, Stratigraphy	26-Jan	BF1, BF2, UF1, SNOWEX
9-Feb	Density, Temperature, Stratigraphy	7-Feb	BF1, BF2, UF1, SNOWEX
21-Feb	Density, Temperature, Stratigraphy	26-Feb	BF1, BF2, UF1, SNOWEX
7-Mar	Density, Temperature, Stratigraphy	9-Mar	BF2, UF1, SNOWEX
21-Mar	Density, Temperature, Stratigraphy, LWC	14-Mar	BF1; SfM
4-Apr	Density, Temperature, Stratigraphy, LWC	23-Mar	BF1, BF2, UF1, SNOWEX
17-Apr	Density, Temperature, Stratigraphy, LWC	6-Apr	BF1, BF2, UF1, SNOWEX
7-May	Density, Temperature, Stratigraphy, LWC	16-Apr	BF1; SfM
19-May	Density, Temperature, Stratigraphy, LWC	6-May	BF2, UF1, SNOWEX
26-May	Density, Temperature, Stratigraphy, LWC	19-May	BF1, BF2, UF1, SNOWEX
3-Jun	Density, Temperature, Stratigraphy, LWC	26-May	BF1, BF2, UF1, SNOWEX; SfM
-	-	3-Jun	BF1, BF2, UF1, SNOWEX
-	-	13-Jun	BF1, BF2, UF1, SNOWEX

### **3.1.3 Snow Surface Albedo Measurements**

I programmed the paired AWS to collect incoming and outgoing shortwave radiation and albedo every minute and store the average fifteen-minute and sixty-minute values. To determine daily albedo, I calculated the median hourly albedo between 1000–1400 for each date at both weather stations. By taking the median over this time range and applying a 7-day smoothing function, I reduced noise in the measured albedo at the unburned AWS which was caused by canopy interception of incoming radiation creating diffuse light at the sensor.

I also collected spectral albedo observations in the burned forest and an open unburned meadow near the burned and unburned AWS sites in clear-sky conditions on 15 May. I used a Malvern Panalytical/Analytical Spectral Devices FieldSpec 4 Standard-Res spectroradiometer (3 nm VNIR, 10 nm SWIR resolution) at six locations evenly split between the burned area and the unburned area. At each of the six locations, five upward and five downward measurements were taken within 2 hours of solar noon using the ASD remote cosine reflector on an outstretched 60 cm metal arm to the south of a tripod. Each of the five manually triggered observations collected five automated measurements. I calculated albedo as the ratio of the upwelling and downwelling measurements and is presented as the mean albedo at the burned and unburned sites.

## **3.2 Data Processing**

### **3.2.1 Snow Water Equivalent Calculations**

Using the density profiles, I calculated the bulk snow density at each snow pit. Combining the bulk pit densities with density from the six SWE tube locations, I calculated the mean density for each aspect and burn condition. Bulk snowpack density was then linearly interpolated between sampling dates to assume daily bulk density. I then calculated mean daily

SWE for each aspect and burn condition by multiplying the daily bulk density by the continuous snow depth measurements. The mean daily SWE was then calculated for each aspect and burn condition. A similar procedure was used to calculate daily transect SWE, but no linear interpolation was needed to calculate the SWE for each of the 16 transect data collection dates.

### 3.2.2 Terrain Analysis and Cold Content

As a measure of terrain complexity within the burned seasonal snow zone and across all sites and distributed snow depth transect points, I calculated northness (Molotch et al., 2005),

$$Northness = \cos(aspect (^{\circ})) \times \sin(slope\ angle (^{\circ})) \quad (1)$$

In this work, I used a preliminary USGS LiDAR derived DEM with a 0.7 m spatial resolution and calculated slope angle, topographic aspect, and northness using QGIS Raster Tools. While the 0.7 m resolution DEM was used in all analysis, I down-sampled the northness raster to 10 m resolution for clarity in Figure 4.

Cold content is a measure of the snowpack energy deficit, which depends on the snowpack's temperature and mass. This deficit must be overcome before snowmelt runoff can occur. I calculated cold content for each study site as:

$$CC = c_i \rho_s d_s (T_s - T_m) \quad (2)$$

where  $CC$  is the snowpack cold content ( $\text{MJ m}^{-2}$ ),  $c_i$  is the specific heat of ice ( $2.1 \times 10^{-3} \text{ MJ kg}^{-1} \text{ }^{\circ}\text{C}^{-1}$ ),  $\rho_s$  is the density of snow ( $\text{kg m}^{-3}$ ),  $d_s$  is snow depth (m),  $T_s$  is the depth weighted snowpack temperature ( $^{\circ}\text{C}$ ), and  $T_m$  is the melting temperature of snow ( $0 \text{ }^{\circ}\text{C}$ ). Due to the north burned site having a likely positive bias in snow depth due to wind drifting, I calculated cold content using the median distributed snow depth in each burn condition (burned/unburned) and aspect (north/south) instead of snow pit depth. Snow density was calculated as the mean bulk

snow density per each snow pit. Snowpack temperature was measured at the snow surface and every 10 cm in each snow pit profile.

### 3.3 Snowpack Energy Balance

Using the burned and unburned AWS measurements, I calculated the total energy balance for each site using a simple one-directional model:

$$Q = K + L + H + L_v E + R + G \quad (3)$$

where  $Q$  is the total energy available,  $K$  is the net shortwave radiation,  $L$  is the net longwave radiation,  $H$  is the sensible heat flux, and  $L_v E$  is the latent heat flux. All terms have units of  $\text{W m}^{-2}$ . The energy inputs from rainfall ( $R$ ) and the ground heat flux ( $G$ ) were not included since no rain was observed during the observational period, and the ground heat flux is assumed to be negligible (Boon, 2009).

#### 3.3.1 Shortwave and Longwave Components

For each site I calculated  $K$  and  $L$  from the mean hourly observations using:

$$K = K_{in} - K_{out} \quad (4)$$

and,

$$L = L_{in} - L_{out} \quad (5)$$

where  $K_{in}$  and  $L_{in}$  are the incoming radiation components ( $\text{W m}^{-2}$ ), while  $K_{out}$  and  $L_{out}$  are the outgoing radiation components ( $\text{W m}^{-2}$ ). Hours with incoming shortwave radiation less than outgoing shortwave radiation were removed since these are not physically realistic and are mainly due to snow covering the upward-looking sensor. Additionally, 17 days with less than six hours of shortwave data were removed, most days in the record had more than 8 hours of shortwave data.

### 3.3.2 Turbulent Energy Flux Modeling

I measured wind speed at two locations, the burned AWS and the unburned AWS. Wind speed and air temperature were only measured 3 m above the ground surface at the burned and unburned sites. I extrapolated wind speeds and air temperatures to the daily height of the snow surface to calculate the sensible and latent heat fluxes (Boon, 2009; Mandal et al., 2022).

For each of the sites, hourly  $H$  and  $L_vE$  were calculated as a function of the temperature, vapor pressure, and wind speed gradients above the surface of the snow,

$$H = \rho_a C_p D_H (T_a - T_{ss}), \quad (6)$$

$$L_vE = \rho_a \lambda_v D_E \frac{0.622}{P} (e_a - e_s), \quad (7)$$

where  $\rho_a$  is the air density at the sites ( $\text{kg m}^{-3}$ ),

$$\rho_a = \frac{0.34722 \times P_a}{T_a}, \quad (8)$$

where  $P_a$  is the air pressure (mbar) at each site. Since air pressure was only recorded at the burned AWS and both sites are in close proximity and at similar elevations, the burned AWS air pressure was used at both sites. The specific heat capacity of air ( $C_p$ ) was set as  $1005 \text{ J kg}^{-1} \text{ K}^{-1}$  and  $P$  is the site pressure in kPa.  $T_a$  is the air temperature ( $^{\circ}\text{K}$ ) and the snow surface temperature ( $T_{ss}$ ;  $^{\circ}\text{K}$ ) was calculated using,

$$T_s = \left( \frac{L_{out}}{\varepsilon_s \sigma} \right)^{\frac{1}{4}}, \quad (9)$$

where the emissivity ( $\varepsilon_s$ ) of the snow surface is assumed to be 0.97 (Hardy et al., 1997), and  $\sigma$  is the Stefan-Boltzmann constant ( $5.67 \times 10^{-8} \text{ W m}^{-2} \text{ K}^{-4}$ ).

The latent heat of vaporization ( $\lambda_v$ ;  $\text{MJ kg}^{-1}$ ) was given by,

$$\lambda_v = 2.501 - 0.002361(t_{ss}), \quad (10)$$

where  $t_{ss}$  is the snow surface temperature in degrees Celsius.

Using Teten's formula (F. W. Murray, 1967), I calculated the saturation vapor pressure of the air ( $e_{a_{sat}}$ ) and the snow surface ( $e_{s_{sat}}$ ) in kPa,

$$e_{a_{sat} \text{ or } s_{sat}} = \begin{cases} 6.11 \times \exp\left(\frac{17.27t_{a \text{ or } ss}}{t_{a \text{ or } ss} + 237.3}\right); & t_{a \text{ or } ss} > 0^\circ\text{C} \\ 6.11 \times \exp\left(\frac{21.87t_{a \text{ or } ss}}{t_{a \text{ or } ss} + 265.5}\right); & t_{a \text{ or } ss} \leq 0^\circ\text{C} \end{cases}, \quad (11)$$

where  $t_{a \text{ or } ss}$  is either the air temperature ( $t_a$ ) or snow surface temperature ( $t_{ss}$ ) in degrees Celsius. We assumed the snow surface vapor pressure ( $e_s$ ) was always saturated, giving  $e_s = e_{s_{sat}}$ , but to determine the air vapor pressure ( $e_a$ ), I used,

$$e_a = \frac{RH}{100\%} \times e_{a_{sat}}, \quad (12)$$

where  $RH$  is the hourly measured relative humidity (%) at each AWS site.

Finally,  $D_H$  and  $D_E$  are the bulk transfer coefficients of sensible and latent heat ( $\text{m s}^{-1}$ ). Under neutral atmospheric conditions  $D_H$  and  $D_E$  are assumed to be equivalent to each other and calculated as:

$$D_H = D_E = \frac{k^2 u}{\left[\ln\left(\frac{z_u}{z_0}\right)\right]^2}, \quad (13)$$

where  $k$  is the von Karman constant (0.4) and  $z_0$  is the roughness length (m). Due to a lack of field measurements, I assumed all roughness lengths to be 0.006 m following (Boon, 2009). The wind speed measurement height ( $z_u$ ) is the height (m) above the snowpack at each site.

To account for the stability of the surface boundary layer and correct the turbulent fluxes under highly variable conditions I used the Richardson number ( $R-i$ ; Brutsaert, 1982):

$$R_i = g \frac{(T_a - T_{ss}) z_u}{T_a u^2}, \quad (14)$$

where  $g$  is gravitation acceleration ( $9.81 \text{ m s}^{-2}$ ),  $u$  is the hourly average wind speed ( $\text{m s}^{-1}$ ) measured at each site. Due to substantial variability, potential hysteresis, and a wide-range in published values and approaches in the determination of the  $R_i$  critical number (Andreas, 2002), and a sizable portion of the  $R_i$  values falling below zero, turbulence was dampened when  $R_i$  was not between  $-0.4$  and  $0.3$  (Andreas, 2002; Boon, 2009; Mandal et al., 2022). The turbulence was dampened for stable atmospheric conditions using,

$$D_{Hc} = D_{Ec} = \frac{D_H}{(1 + 10R_i)}. \quad (15)$$

## 4. RESULTS

I begin by addressing my first two research questions using the in-situ data collection to address how wildfire burned areas alter i) the quantity and date of peak SWE, and ii) the ablation patterns across complex terrain. Then, using the paired burned and unburned AWS data, I will compare the net energy balance within an area highly impacted by wildfire and one that is representative of the forest not impacted by wildfire, answering my final research question.

### 4.1 Influence of Complex Terrain

#### 4.1.1 Quantity and Timing of Peak SWE

While bulk snowpack density exhibited similar temporal trends on all aspects throughout the observation period, density in burned areas was an average 10% greater than at the unburned sites on north aspects and 15% greater in the burned south aspects compared to unburned south areas (Figure 6a). Beginning 21 February, snowpack density on the burned south aspect was greater (0.4–12%) than the north burned aspect for all subsequent dates other than 26 May (Figure 6a). This differed from the unburned aspects where there was more variability in what aspect had greater density throughout the observational period.

SWE was greater on north aspects in both burned and unburned areas than on south aspects during the first survey (14 November; burned 101% increase; unburned 95% increase) and this trend persisted throughout the accumulation period (Figure 6b and Figure 6c). North aspects had more SWE in both burned and unburned locations throughout the accumulation period with SWE greater in burned areas than unburned areas on both aspects on all dates except 28 November and 28 December on south aspects (Figure 6b and Figure 6c). However, the difference between median SWE in burned and unburned areas was only significantly different

(Wilcoxon t-test;  $p < 0.05$ ) during the accumulation period on 28 December on north aspects, while significant differences occurred on south aspects on four survey dates (Figure 6b and Figure 6c). During accumulation, the majority of aspects and burn conditions had comparable SWE to the median distributed SWE measurements. The one exception was the burned north aspect (camera) site had a consistent positive bias (25% median difference), likely due to wind deposition or an increased amount of early season persistent snow deposition (Figure 6b and Figure 6c). Additionally, I found the difference in median interquartile range (IQR) of SWE was significantly greater ( $p < 0.05$ ) on north burned aspects than north unburned areas, and greater on north than south aspects within the burned area during accumulation.

The mean continuous burned south aspect site (Burned-South Camera) reached peak SWE on 15 April (413 mm), while the other three sites reached peak SWE on 7 May (22 day difference; Figure 6b and Figure 6c). On 6 May, distributed snow depth on the north burned transect points had accumulated 19 mm (3%) more SWE than north unburned sites, while south burned aspects had 34 mm (9%) less SWE than unburned south sites (Figure 6b and Figure 6c). When comparing 6 May unburned south aspect SWE to 6 April burned south aspect SWE, the nearest distributed measurement day to 15 April peak SWE, the burned site had 9 mm (2%) greater peak SWE. None of these differences are significantly different when evaluated with a Wilcoxon test of difference in medians ( $p < 0.05$ ). Between peak SWE on the burned south aspect and peak SWE at all other aspects (yellow period in Figure 6b and Figure 6c), the south aspect burned area was losing SWE at  $4 \text{ mm d}^{-1}$ , while burned north and unburned north and south were gaining SWE at 2, 3, and  $1 \text{ mm d}^{-1}$ , respectively.

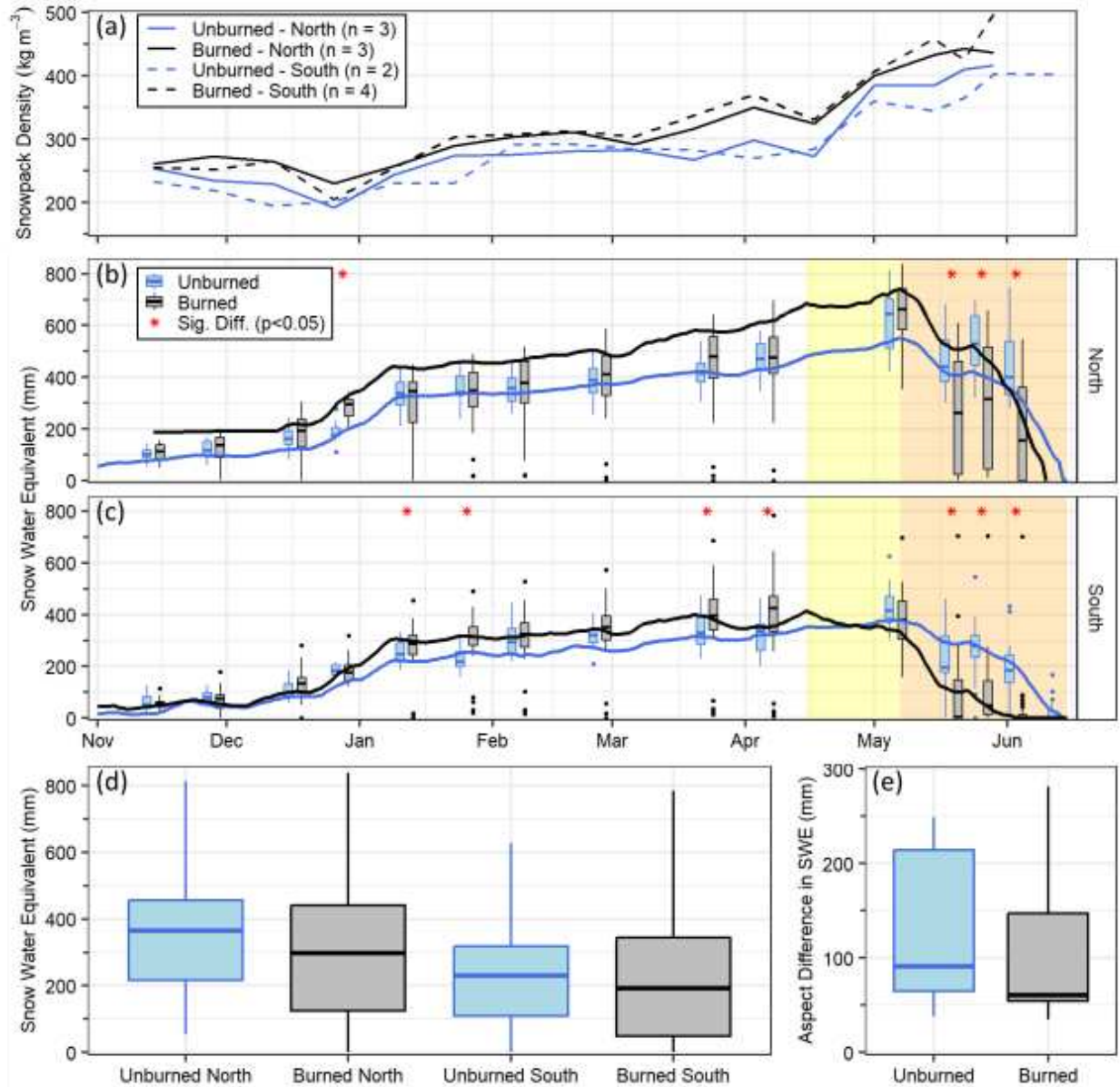


Figure 6. Average density for each aspect and burn condition calculated from the mean snow pit bulk density and SWE tube densities (a). The number of sites included for each aspect and burn condition is included in the legend. Distributed and continuous SWE based on burn condition for north (b) and south (c) aspects. Wilcoxon significant differences ( $p < 0.05$ ) between burned and unburned areas are indicated with the red asterisks. Yellow indicates the period between burned south peak SWE (15 April) until peak SWE on all other sites (7 May). The melt period for all sites is shown in orange. The mean continuous SWE measurements include two sites for all aspects and burn conditions except for the burned north which has one site. Boxplot of distributed snow water equivalent calculated from transect depth and pit density (d). Significant differences ( $p < 0.05$ ) in median occurred between burned and unburned north aspects, and north and south aspects when controlling for burn condition. Aspect differences in SWE (north minus

south) for burned and unburned areas (e). There was no significant difference between burned and unburned south aspects or between burned and unburned aspect differences.

#### 4.1.2 Melt Rates and Timing

The differences between the burned and unburned sites were particularly acute during the melt period. Between peak SWE (7 May for most aspects and burn conditions) and 20 May, when a five-day, ~30 cm storm began, the mean SWE melt rate on the burned north and south sites were both  $19 \text{ mm d}^{-1}$  (Figure 7). During this same period, mean SWE loss on unburned north and south aspects was 12 and  $8 \text{ mm d}^{-1}$ . In comparison, the SWE loss was 61% and 147% greater in the burned area for north and south aspects, respectively. Between the end of the storm and burned south SDD, burned north and south aspects lost SWE at  $19$  and  $8 \text{ mm d}^{-1}$ , while the unburned north and south aspects lost SWE at  $8$  and  $8 \text{ mm d}^{-1}$ .

The early discrepancies in melt rates following peak SWE created pronounced differences in SWE between different aspects in the burned and unburned sites (Figure 6b and Figure 6c). Between 19 May and 3 June, the median difference between burned and unburned sites was 213 mm on north aspects and 191 mm on south aspects. While differences between comparable aspects in the burned and unburned areas were similar during this period, the median SWE was 0–49 mm on burned south aspects but was 157–316 mm on burned north aspects. During the melt period, the IQR expanded considerably on burned north aspects (Figure 6b), with the burned north IQR growing 246 mm (78%) greater than the IQR on unburned north aspects. Burned south IQR was 32 mm (29%) greater than comparable unburned areas. Due to the limited number of survey dates (3), neither change in IQR is statistically significant.

Snow disappearance occurred on south burned aspects 3 June and on north burned aspects on 10 June, all unburned areas became snow free on 14 June (Figure 6). The steeply

sloped south aspects (low northness) were snow free on 19 May, prior to the five-day spring snowstorm, and became snow free for the season on 1 June after a few additional small storms in late May.

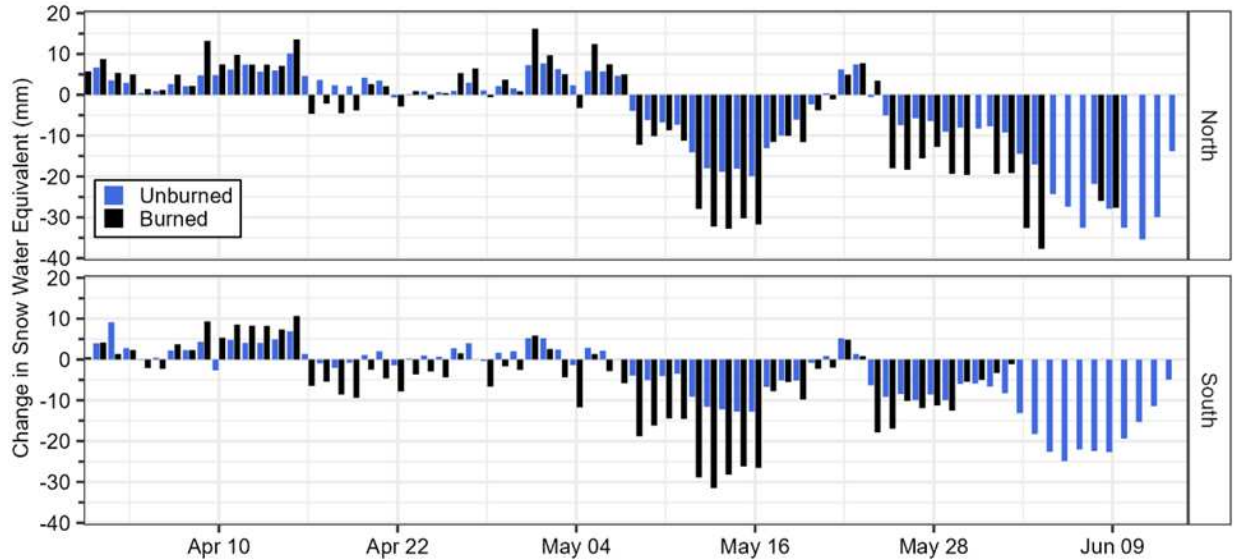


Figure 7. Daily change in SWE based on slope aspect and burn condition. Mean melt rates are calculated for each aspect from peak SWE on most aspects (7 May) through the beginning of a mid-May snowstorm (20 May) and from 25 May to burned south SDD on 3 June.

## 4.2 Snowpack Preconditioning Following Wildfire

Snowpack cold content exhibited a distinctive seasonal pattern during the observational period, with an increase in cold content from November through January. Maximum cold content occurred at all sites in early February, followed by a decline until all sites reached isothermal conditions in early May (Figure 8). Cold content was greatest on the north burned aspect through 27 December, while the other three sites were similar (Figure 8). Beginning with the 24 January survey, cold content showed greater similarities based on aspect rather than burn condition, with the north aspects containing greater cold content than south aspects (Figure 8). Aspect-driven similarities continued until 21 March when snowpack cold content in the burned areas decreased

at a greater rate than unburned areas. All locations were isothermal during the 7 May survey (Figure 8).

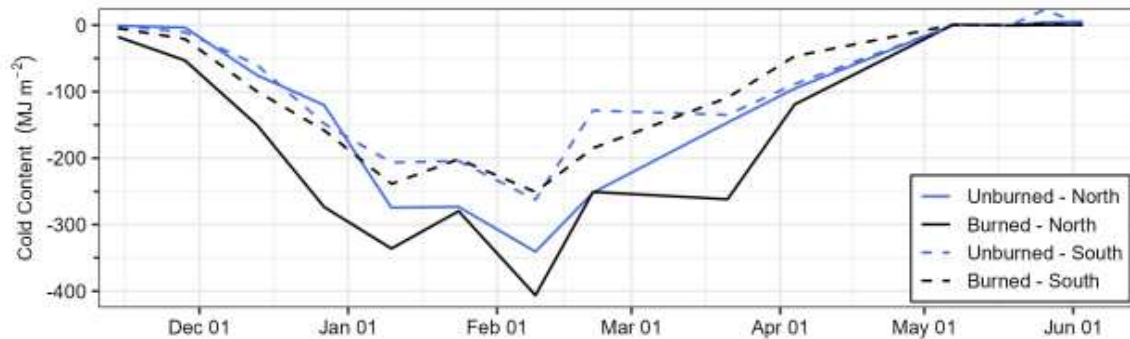


Figure 8. Timeseries of the mean snowpack cold content based on aspect and burn condition. Cold content was calculated using the mean density, weighted average temperature, and median distributed snow depth per aspect and burn condition.

### 4.3 Wind Speed Following Wildfire

Wind speeds in the burned areas were increased with comparison to the unburned AWS. The burned AWS recorded median seasonal windspeeds of  $1.76 \text{ m s}^{-1}$  while the wind speeds at the unburned AWS were significantly lower ( $p < 0.05$ ;  $0.45 \text{ m s}^{-1}$ ; Figure 9a). At the burned AWS, 40% of all hourly windspeeds were greater than  $2 \text{ m s}^{-1}$  while there were no occurrences greater than  $2 \text{ m s}^{-1}$  at the unburned AWS (Figure 9b and Figure 9c). The predominant wind directions were similar (south-southwest) at both sites (Figure 9b and Figure 9c).

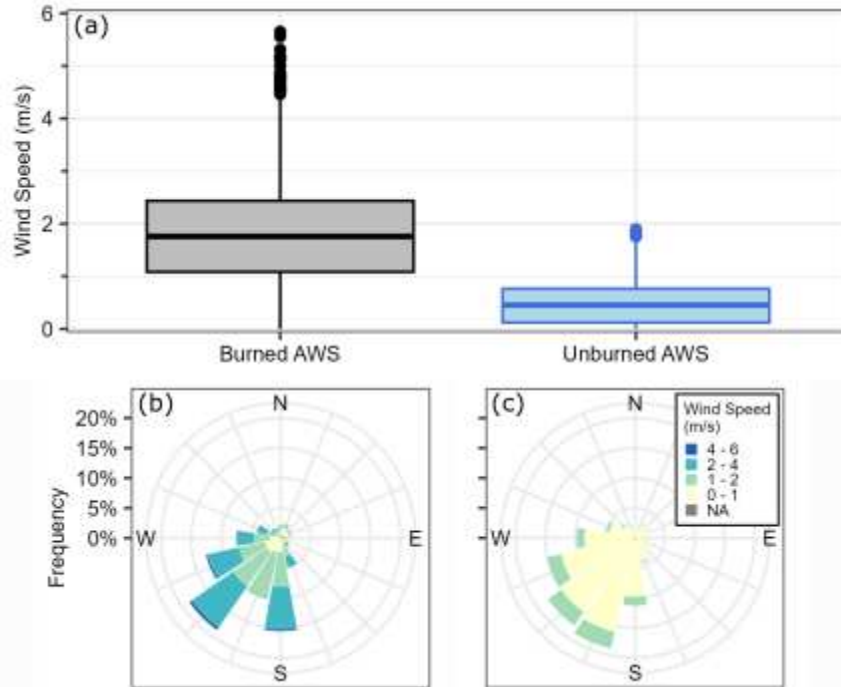


Figure 9. Boxplot of hourly wind speed at the burned and unburned automated weather stations between mid -November and mid-June (a). The median windspeed at the burned AWS was statistically greater (Wilcoxon;  $p < 0.5$ ) than the unburned AWS. Wind rose showing hourly windspeed and direction for each weather station, Burned AWS (b) and Unburned AWS (c).

#### 4.4 Energy Balance Following Wildfire

Due to wildfire directly changing the canopy and forest structure, all aspects of the snowpack energy balance are greatly altered following wildfire. Below I present results for the energy balance components based on observations from the burned and unburned AWS sites.

##### 4.4.1 Shortwave Radiation Balance

I observed significant increases (Wilcoxon t-test;  $p < 0.05$ ) in shortwave radiation within the burned area relative to the unburned site over the full observation period (Figure 10a). However, the magnitude of the increase in net shortwave radiation at the burned site varied seasonally, with a greater increase in the spring than in mid-winter. Focusing on a mid-winter period (1 December–1 February) and a spring timeframe prior to melt (1 April–1 June), we

found that the percent increase of median daily incoming shortwave radiation at the burned site compared to the unburned was 190% and 213%, respectively. However, due to the longer days and increased zenith angle, there was ~220% more cumulative incoming shortwave energy at both sites during the spring period than during mid-winter. This consistent increase in incoming shortwave radiation and a decrease in the snow surface albedo due to soot and ash from the burned canopy altered significantly ( $p < 0.05$ ) altered the net shortwave radiation during both the mid-winter and spring periods (Figure 12a). During the mid-winter, median daily net shortwave energy at the burned site ( $395 \text{ W m}^{-2}$ ) was 73% greater than the unburned site ( $228 \text{ W m}^{-2}$ ), but during the spring this difference increased to 165% greater at the burned site ( $2.1 \text{ kW m}^{-2}$ ) than the unburned site ( $799 \text{ W m}^{-2}$ ; Figure 12a). In total, there was a 137% increase in cumulative net shortwave radiation throughout the observation period (late November–early June) at the burned site relative to the unburned site.

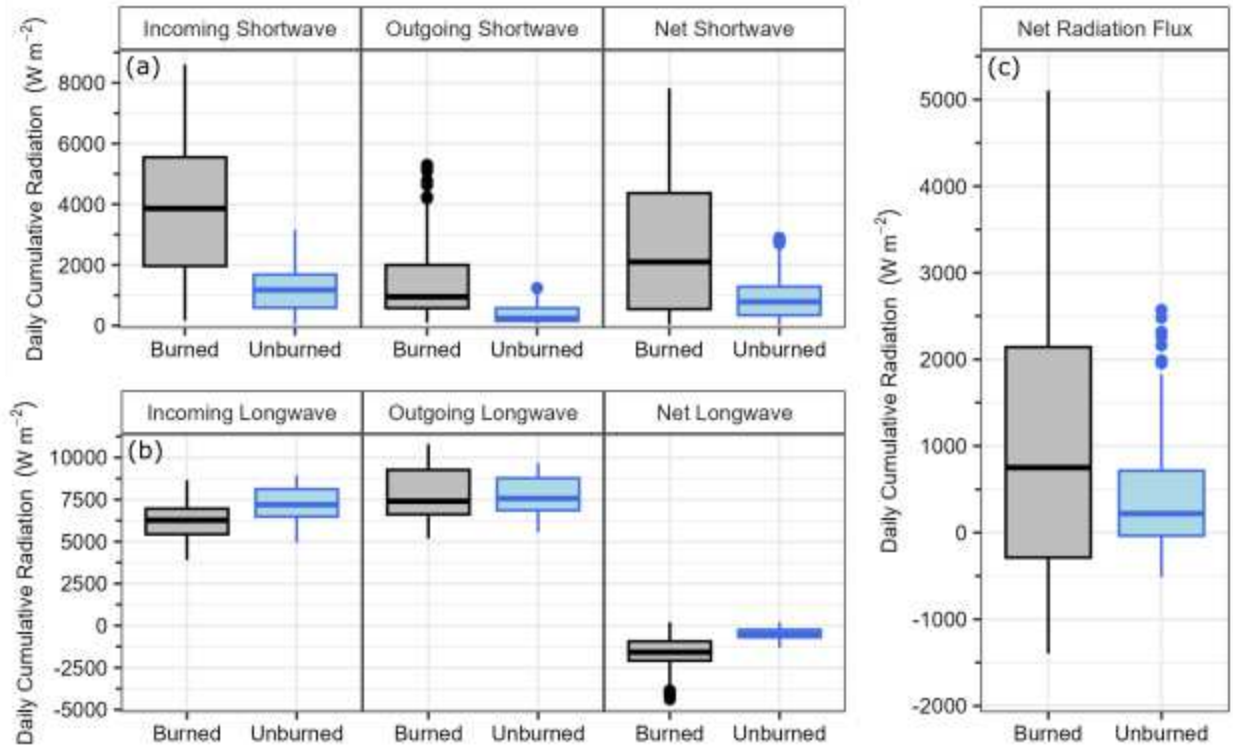


Figure 10. Daily cumulative incoming, outgoing, and net shortwave (a) and longwave radiation (b), and net radiation flux (c) for the burned and unburned AWS sites. Wilcoxon statistical difference in medians determined significant differences ( $p < 0.05$ ) between the burned and unburned sites for all radiation fluxes except outgoing longwave radiation.

#### 4.4.1.1 Snow Surface Albedo

The darkening of the surface albedo in the burned area was a key component of the shortwave energy balance. I found the broadband albedo (upward-looking, 385 nm to 2105 nm; downward-looking, 295 nm to 2685 nm) at the unburned AWS was approximately 49% lower than the albedo from the burned area AWS on 15 May (Figure 11a). I believe the burned site observations indicate a greater albedo than the unburned site even though the snow surface in the burned area was visibly darker to be due to a difference in the way energy was being dispersed through the unburned canopy. Since the canopy is gone at the burned site, the incoming shortwave radiation was not dispersed. The dispersed incoming energy at the unburned site

resulted in the measured albedo in the forest to be lower than in the open burned site. A better comparison of time series albedo would be in an open area or a less dense canopied site where the measurement of albedo would be more comparable between the two sites. On 15 May, we found the spectral albedo in the burned area was 37% less ( $p < 0.05$ ) than the spectral albedo in the unburned areas across all measured wavelengths (350–2500 nm; Figure 11b). In the visible wavelengths (400 – 700 nm), we found there to be a significant difference ( $p < 0.05$ ) in the median albedos—the burned area albedo (0.44) was 73% less than the unburned area albedo (0.76). In the measured NIR spectrum (700 – 2500 nm), the burned area median albedo (0.14) was 26% less ( $p < 0.05$ ) than the unburned area (0.19). Prior to the 15 May spectral albedo measurements, a snowstorm carrying dust darkened the surface of all sites (Figure 11c and Figure 11d), however, the debris and soot from the remaining burned forest darkened the snow surface further.

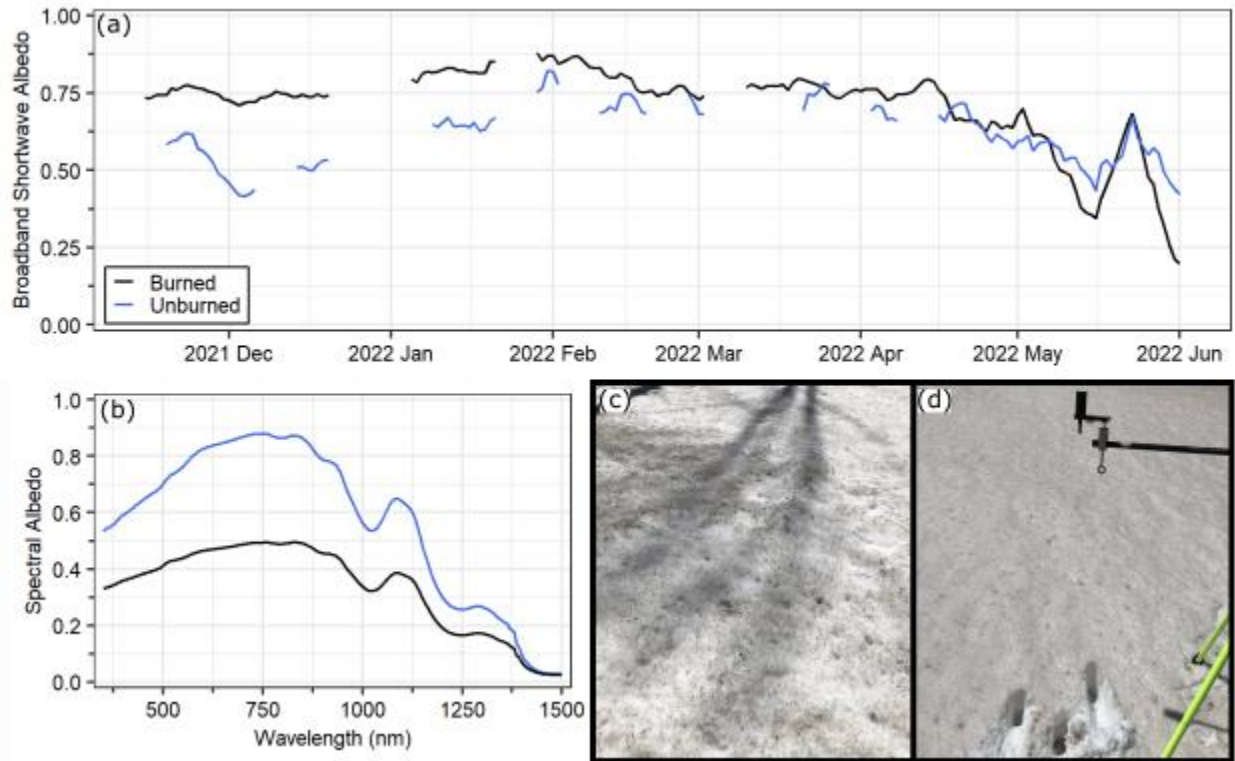


Figure 11. Seven-day smoothed timeseries of broadband (upward-looking, 385 nm to 2105 nm; downward-looking, 295 nm to 2685 nm) albedo at the burned and unburned automated weather stations. Albedo was calculated as the median value between 1000 and 1400 (a). Spectral albedo in burned and unburned locations on 15 May 2022 (b). Burned area snow surface on 15 May in the area where one ASD measurement location occurred (c). Unburned snow surface and the ASD remote cosine receptor and tripod on 15 May (d). Note: Snow samples were taken after all measurements were collected.

#### 4.4.2 Longwave Radiation Balance

Post-fire, incoming longwave radiation was lower in the burned area compared to the unburned area. The difference was similar throughout the observation period, with a significant ( $p < 0.05$ ) mid-winter difference of 18% and a spring difference of 13%. Outgoing longwave radiation at the burned site was also lower than the unburned site, however the magnitude of the decrease was smaller during both the winter (5%) and spring (1%) seasons. As a result, median daily net longwave radiation was consistently ~200% ( $p < 0.05$ ) more negative at the burned site than at the unburned site (Figure 5a and Figure 5b).

#### **4.4.3 Net Radiation Balance**

From the beginning of the analysis (late November) through mid-March, net radiation flux was negative on approximately two-thirds of the days at both the burned (64% of days) and unburned (72% of days) AWS sites (Figure 12a and Figure 12b). However, from 20 November to 15 March, the magnitude of net radiation was more negative at the burned site than the unburned AWS, indicated by a median  $-118\%$  daily difference and a daily difference IQR of  $-97$  to  $-165\%$  (Figure 12f). Between 1 December and 1 February, the cumulative daily net radiation at the burned site was  $46 \text{ kW m}^{-2}$  (361%) less than the unburned site. As the length of day and solar zenith angle increased through March, the daily net radiation flux at the burned site became consistently positive by late March and remained so until complete snow disappearance (Figure 12a). From 1 March until 1 May, the burned site received a cumulative  $28 \text{ kW m}^{-2}$  (361%) more net radiation than the unburned site. While the early season cumulative net energy was significantly decreased at the burned site, the spring energy balance drove increased daily net radiation fluxes. This seasonality of net energy led to a significant ( $p < 0.05$ ) 246% increase in median daily net radiation at the burned site over the unburned location between late November and burned seasonal snow disappearance in early June (Figure 10c).

#### **4.4.4 Turbulent Heat Fluxes**

The differences in wind speed observed between the burned and unburned AWS sites resulted in considerable increases in the magnitude of sensible and latent heat fluxes in the burned area compared to the unburned AWS (Figure 12d and Figure 12e). At both sites the sensible heat flux was primarily positive (burned 66%; unburned 64%) throughout the whole

period, however the median daily flux increased from  $1.5 \text{ W m}^{-2}$  at the unburned site to  $220 \text{ W m}^{-2}$  at the burned site. These vast differences in the magnitude of the sensible heat flux caused a cumulative total of  $6.1 \text{ kW m}^{-2}$  to be added to the burned site while the unburned site lost  $475 \text{ W m}^{-2}$ . The burned site experienced an increase in the frequency and magnitude of negative latent heat fluxes. From 1 December through complete snowmelt at the burned site (3 June), the latent energy balance was negative 73% of the days at the unburned site while the burned site experienced negative latent heat fluxes 98% of days. Like the sensible heat flux, the magnitude of latent heat was substantially greater at the burned site (median value of  $-805 \text{ W m}^{-2}$  at the burned site vs  $-45 \text{ W m}^{-2}$  at the unburned site). Both sensible and latent heat fluxes varied considerably throughout the season with the lowest magnitude sensible and latent heat fluxes occurring during periods of snow fall and the greatest values occurring during periods of high pressure. Sensible and latent heat fluxes typically have opposite directions of heat transfer, causing the magnitude of the cumulative of turbulent flux to be less than the sensible and latent heat components alone. In the burned area, the median daily turbulent flux increased from  $-47 \text{ W m}^{-2}$  at the burned site to  $-582 \text{ kW m}^{-2}$ . This difference in the median daily median lead to an increased magnitude of the cumulative turbulent energy at the burned site ( $-141 \text{ kW m}^{-2}$ ) compared to the unburned site ( $-24 \text{ kW m}^{-2}$ ).

#### **4.4.5 Net Energy**

The daily net energy ( $Q$ ) at both the burned and unburned sites was consistently negative through the accumulation period and into the spring. The direction of the daily net energy flipped to persistently positive at the unburned site on 13 April and at the burned site on 1 May (Figure 12f). Prior to this sign change, between 20 November and 13 April, the median daily net

energy was  $-1.1 \text{ kW m}^{-2}$  and  $-0.2 \text{ kW m}^{-2}$  at the burned and unburned sites. Additionally, over this period the burned site accumulated a 390% increase in net energy deficit than the unburned site. Before 13 April the differences between burned and unburned areas was primarily due to changes to the net longwave and turbulent flux components of the energy balance (Figure 12g). The primary component of the difference between the burned and unburned sites then became the net shortwave radiation through April and May, causing the net energy at the burned site to become greater than at the unburned site (Figure 12g). Due to this increasing shortwave radiation, after May 1, the cumulative radiation balance was 22% greater at the burned site than the unburned site.

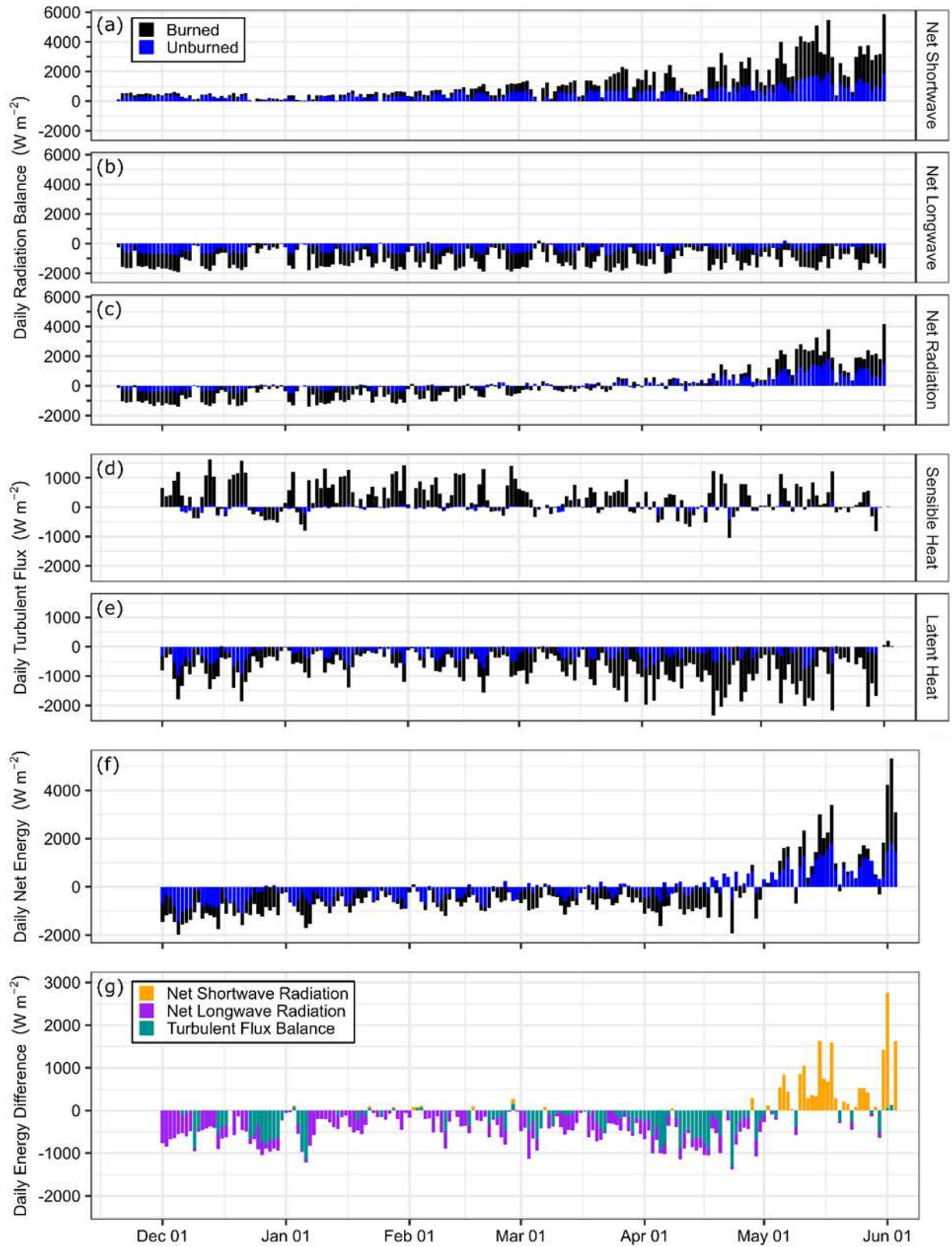


Figure 12. Daily cumulative net shortwave (a), longwave (b), and radiation flux (c) for the burned and unburned AWS sites. Daily cumulative sensible (d) and latent (e) turbulent heat fluxes for the burned and unburned AWS sites. Net energy at the burned and unburned AWS sites (f). Daily difference between the net energy at the burned and unburned sites (burned minus unburned), and the proportion of the net difference attributed to each energy flux (g).

## 5. DISCUSSION

### 5.1 Snowpack Accumulation and Melt

#### 5.1.1 Peak SWE Timing and Quantity

I found that the alterations to the timing and quantity of peak SWE within the burned areas were dependent on the topographic aspect of the study site, with burned south aspects more greatly impacted than north aspect areas. Comparing distributed peak SWE from the probe surveys on 6 May, one day prior to peak SWE at most of the automated stations, I found no significant difference in SWE between burned and unburned areas on both north and south aspects (Figure 14). These results differ from previous western U.S. studies which have reported decreases of 10 to 50% in peak SWE within burned areas (Giovando & Niemann, 2022; Harpold et al., 2014; Smoot & Gleason, 2021), or the 2020–2021 winter at the same study area and burned area where peak SWE in burned areas decreased by 17–25% (Kampf et al., 2022; McGrath et al., 2023). Discrepancies in peak SWE between the 2020–2021 and 2021–2022 winters within the Cameron Peak fires area highlights interannual variability in snow accumulation patterns of the western U.S. and suggests that the changes in energy and mass balance due to wildfire accentuate these interannual differences. The timing of peak SWE was highly dependent on the topographic aspect within the burned areas, with south aspect burned areas peaking 22 days earlier than unburned south aspects. North burned aspects peaked concurrently with the unburned areas. The 22 day advance in peak SWE date on south aspects is far greater than the 6-to-10 day averages reported in previous literature for the western U.S. and Southern Rockies (Giovando & Niemann, 2022; Smoot & Gleason, 2021). In contrast to the differences in peak SWE between the 2020–21 and 2021–22 winters in this study area, the change in SDD between burned and unburned areas was consistent between the years (11–13

days; McGrath et al., 2023), and were similar to the average for the Southern Rockies (11.7 days; Giovando & Niemann, 2022), but are less dramatic than the 23 days reported by (Gleason et al., 2013).

### **5.1.2 Aspect Influence**

Our findings expose key differences based on aspect within burned and unburned locations (Figure 14). Burned south aspects were the most impacted by the wildfire with similar peak SWE to unburned slopes with similar aspects but rapid snow melt rates due to the increased radiative forcing due to increased incoming radiation and decreased surface albedo. North burned aspects also experiences elevated melt rates over unburned north aspects, however due to increases in peak SWE and decreases in the net energy due to less available incoming shortwave radiation, burned north aspects held snow later into the year than south aspects. Due to snowpacks melting earlier on south burned aspects, spatiotemporal variability in wildfire recovery is enhanced by confounding factors of a longer growing season and less soil moisture, lengthening the time needed for vegetation recovery (Webb et al., 2023).

While the north burned aspects were found to hold greater snow depths from the distributed snow depth surveys throughout the entire study period, the dates of in-situ data collection limited understanding the physical processes causing this difference. Using Sentinel-2 and Landsat-8 satellite imagery from the late fall, I determined that an early season snowstorm before 13 October completely melted from burned south aspects by 25 October (Figure 13). Within unburned areas, canopy cover reduces the ability to identify snow, however only steep south unburned aspects show a red signature indicating the loss of snow during this period (Figure 13). While we lack the ability to identify the depth of snow on the ground, this imagery

suggests that snow on the south aspect burn areas completely melted in late October prior to persistent snow accumulating at the end of October. This early season difference in energy balance was observed in the snow depth difference during the accumulation period by the relatively continuous difference in snow depths. Additionally, melt also occurred on unburned low northness aspects, however on aspects where the northness value approached zero (south aspect, low slope), the imagery from 25 October shows that snow did not completely melt in the unburned areas but is gone in the burned areas (Figure 13).

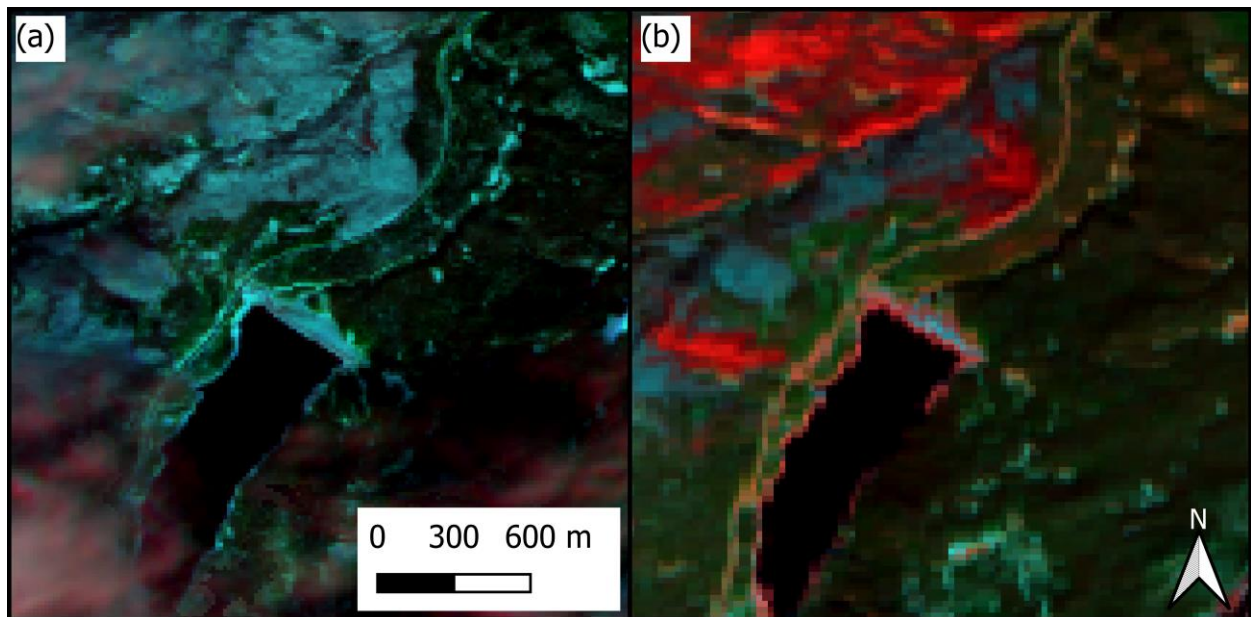


Figure 13. Near-infrared satellite imagery of the Cameron Peak burn site on (a) 13 October (Sentinel-2) and (b) 25 October (Landsat-8). Areas colored in teal are snow covered while areas shown in red are snow free.

## 5.2 Snowpack Energy Balance

While many studies have previously reported the alterations to peak SWE, peak SWE date, melt rates, and SDD, few studies have directly compared the energy balances between burned and unburned sites. I found that incoming shortwave radiation increased by 229%

following the wildfire, driving an increase of 83% in the net radiation budget, while cumulative net shortwave radiation was 137% greater than the unburned site between mid-November and the burned site SDD (Figure 14a and Figure 14b). Unlike net shortwave radiation, the net longwave radiation difference between the burned and unburned sites were consistent throughout the entire study period. Between mid-November and early June, the median daily net longwave radiation decreased by 207% at the burned site compared to the unburned site due to the loss of tree canopy following the wildfire. Due to the seasonal variability in the magnitude of net shortwave radiation differences, the net radiation differences between burned and unburned areas were highly seasonally dependent. This seasonality is highlighted by an increased loss of net radiation in the burned area through the winter, followed by an increased energy gain during spring. These results emphasize the importance of the increased shortwave radiation incident on the snowpack following wildfire in the Southern Rockies, but also that increased longwave radiation losses partially counter this increase, particularly leading up to March. The extreme difference we found in net radiation following 1 March underscores the importance for management solutions that have been shown to reduce the severity of wildfire and improve the likelihood of tree regeneration following the disturbance so that forests regrow, reducing the likelihood of permanent alterations to forest vegetation, particularly on southerly aspects and steep slopes (Davis et al., 2023; Stevens-Rumann & Morgan, 2019). The net turbulent flux was important to the net energy and accounted for a substantial portion of the differences in energy balance between the burned and unburned sites. Throughout the season the net turbulent energy was primarily negative in both the burned and unburned areas indicating but due to the increased magnitude of the latent heat flux which increased sublimation rates in the burned area.

Net energy was always a greater magnitude in the burned site than the unburned site but was a story of two seasons for both the burned and unburned sites with the change in sign occurring at the burned site later than at the unburned site. The daily and cumulative net energy became positive at the burned site approximately 17 days after the unburned site. This difference is driven mainly by the increased loss of net longwave radiation and net turbulent flux requiring additional incoming shortwave energy (longer days, higher zenith angle) to cancel out the energy loss. Additionally, the difference in net energy is seen distinctly in the early season cold content of burned area snowpacks relative to unburned snowpack cold content. In the burned areas, there was greater cold content in the snowpack from the beginning of the observed period until late March when the cold content in the burned areas became greater than the cold content in the unburned areas. The reduced cold content in the early portion of the season could be due to the reduction in longwave energy entering the snowpack from the surrounding live trees and this energy balance persists until the net energy becomes consistently positive in late March when incoming shortwave energy begins to be the most significant portion of the energy balance.

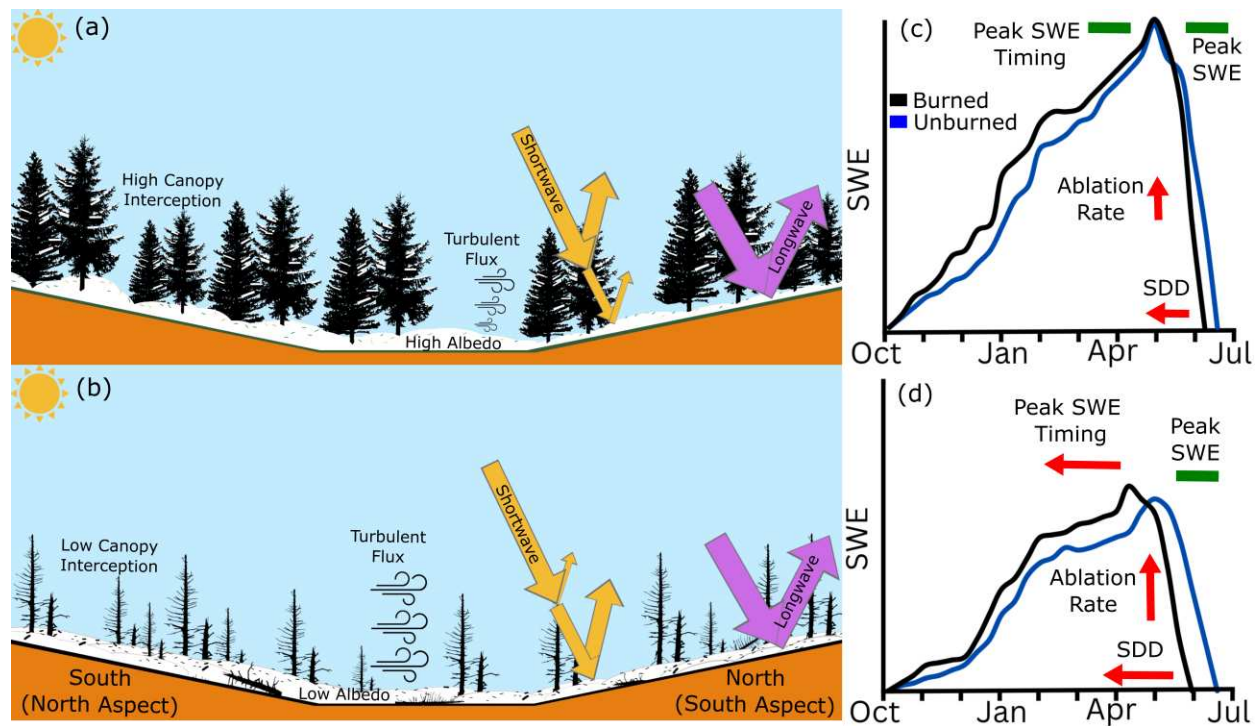


Figure 14. Snowpack energy balance without wildfire (a) and following wildfire (b) based on aspect where arrow and icon size represents relative change. Changes in the snowpack mass balance and timing on north (c) and south (d) burned aspects. Arrow size indicates the magnitude of the change and horizontal bars indicate no change. Black lines indicate burned area and blue lines are unburned areas.

### 5.2.1 Snowpack Albedo

Surface albedo is known to be a primary driver of seasonal snow melt in mid-latitude alpine environments (Painter, Barrett, et al., 2007), due to the direct radiative forcing increases initiated by decreased albedo. Following wildfire, the darkening of the snow surface has been well documented (Burles & Boon, 2011; Gersh et al., 2022; Gleason et al., 2013, 2022; Gleason & Nolin, 2016), and is thought to be a primary driver of the elevated melt rates post-wildfire. Since the unburned station location was in a forested area and primarily received diffuse incoming shortwave radiation, the apparent albedo was biased low compared to the expected albedo values for an unburned site. In contrast, the surface albedo of the burned area appeared

darker relative to unburned areas (Figure 11c and Figure 11d). These shading difficulties add to the list of previously defined complications with in-situ measurements of albedo which can range from issues with instruments not being level ( $< 2^\circ$ ) and issues with differential heating and cooling of the instrument (Michalsky & Hodges, 2013).

Although dust from a 15 April snowstorm event was present at all sites during the 15 May spectral albedo survey, the burned observations yielded a 53% decrease in visible albedo compared to unburned areas. This result is similar to the 40% and 55% decreases identified by (Gleason & Nolin, 2016) and (Hatchett et al., 2023), during melt. This difference in visible albedo was also similar to the 40% found during the first winter following the Cameron Peak fire (McGrath et al., 2023).

Although the 15 April storm brought a considerable amount of dust which eventually accumulated on the surface of the snowpack and darkened the snowpack, the fresh snow first temporarily lowered the surface albedo and slowed the rapid melt. In the burned area, addition of fresh snow during melt could be incredibly important in mitigating the impacts of wildfire since prior to these late season storms the surface albedo is extremely dark from the deposition of soot and debris. Within my study area, there were 12 days from 1 April through SDD with snow depth increases greater than 5 cm, and 5 of the 12 days occurred in May. The quantity of late season events are highly dependent on the ecoregion and the snow persistence zone (Figure 15; McGrath et al., 2023), and the number of events recorded during the 2022 freshet fell within the typical range of the late season snow zone in the Southern Rockies. These observations hint that the occurrence of late season snow could be a driving difference in the reaction to wildfire observed based on the ecoregion and snow zone (Giovando & Niemann, 2022; Smoot & Gleason, 2021). In a changing climate, the number of these late season snow events are expected

to decline, potentially expanding the impacts of wildfire to these locations where the rate of SWE melt was slowed and SDD was delayed due to the addition of late season snow.

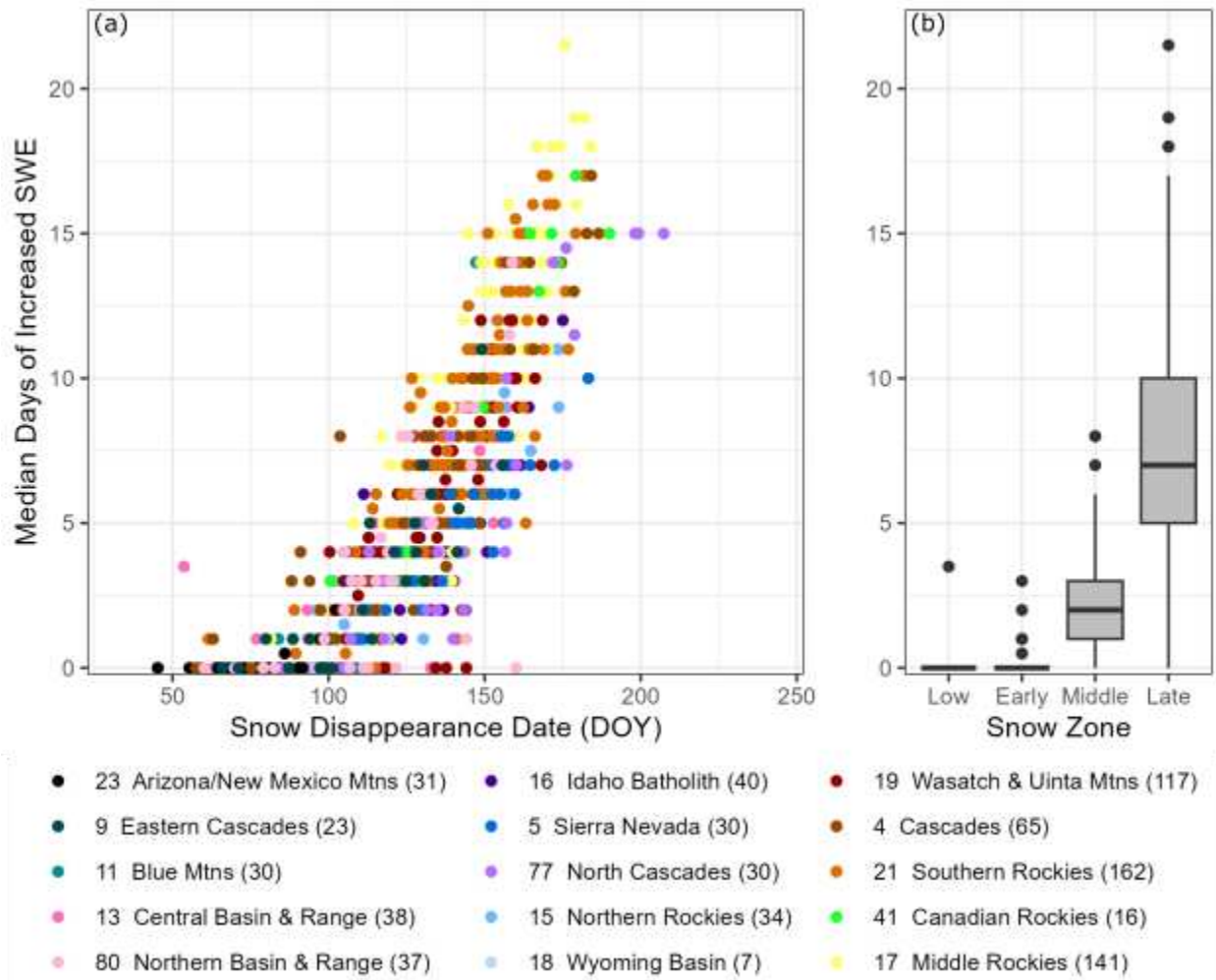


Figure 15. Median number of days after 1 April with increased SWE for each SNOTEL site in the persistent seasonal zone of western U.S. EPA level III ecoregions by mean snow disappearance date (a; O'Leary III et al., 2019). Boxplots of the number of late spring accumulation days for each snow persistence zone defined by (b; Kampf et al., 2022).

## **5.3 Additional Considerations**

### **5.3.1 Influence of Albedo and Pre-wildfire Tree Mortality**

Toward the end of the 2022 melt season, I noted the windward side of most trees were nearly devoid of any black carbon while the leeward aspect was considerably darker (Figure 16a). During this spring period, I also noted that the trees that were not devoid of black carbon on the windward side seemed to have burned more thoroughly during the fire while the ones with little remaining black carbon only burned at the surface (Figure 16a and Figure 16b). I believe this difference in char depth and the availability of black carbon on into the future could be driven by the pre-fire tree health. With trees that were standing dead prior to the fire were burned more deeply while live trees only lost their canopy and sustained superficial burns to the trunk. This plot-scale variability in the availability of black carbon could lead to future scenarios where albedo is highly variable within the burned area depending on the local density of well consumed standing trees. In this scenario, areas with high degrees of consumption will have decreased albedo much longer than other areas with fewer black carbon source trees, potentially creating a mosaic of melt rates and further complicating efforts to predict streamflow from burned areas. While decreased albedo has been detected in burned areas for more than a decade following the fire (Gleason et al., 2019), it is still not well understood how the albedo recovery reacts to local meteorological conditions or pre-fire forest health in the years immediately following wildfire and these observations likely suggest a significant dependence on local wind regimes, the exposure of wind burned slopes to the prevailing wind direction, burn severity, and the efficiency of fuel consumption which may be related to forest mortality prior to the fire.



Figure 16. Photographs of burned trees within the Cameron Peak wildfire burn area with examples of shallow depth burn impacted by wind scour (a) and deeper burn depth (b). Southwest is to the left of photograph (a) and predominate wind direction in the study area is from the southwest. Note trees in the background with highly variable quantities of soot remaining on the trunk.

### 5.3.2 Influence of Snow Zone

In this study I focused on the late snow zone, however the increase in wildfire frequency and burned area observed within the persistent snow zone is also significantly impacting the low, early, and middle snow zones (Kampf et al., 2022). The alterations to these lower elevation snow zones are relatively understudied, so here I attempt to extrapolate the observed alterations to the late snow zone mass and energy balances following wildfire to predict how fire alters the snowpacks in the early and late season snow zones. The low, early, and middle season snow zones are defined by median snow-free dates earlier than 1 March, 1–31 March, and 1–30 April, respectively. In low and early seasonal snow zones, snow typically melts throughout the season while the middle snow zone holds a continuous snowpack throughout the season although it lasts less time than the high-elevation persistent snowpacks.

In high burn severity areas of low, early, and middle snow zones, I expect the increase in shortwave radiation to be similar to the increase observed in the late snow zone, however due to the increased energy available in these lower elevation zones, I would expect the impacts to snowpack processes to be greater than observed in the late season snowpack. Within the low and early snow zones, I predict that the increase in shortwave energy into the snowpack following fire would increase the melt rates, especially on south aspects, and decrease the number of snow-covered days following a snow deposition event. Due to the inherent rapid melt that occurs in these snow zones, the importance of surface albedo in the energy balance will be reduced because any deposition of debris from surrounding trees will end up on the ground soon after the storm due to the periodic melt. Due to this periodic melt throughout the season, low and early snow zones will lack the time required for significant amounts of soot and debris to accumulate on the surface. However, like the late season snow zone, I predict the prolonged existence and melt of the middle snow zone will allow for the accumulation of enough light absorbing particles to alter the surface albedo.

While the albedo may not be altered, the loss of canopy at these lower elevations could lead to more pronounced reductions in length of seasonal snow cover and early initiation of melt due to the warmer temperatures and the lack of canopy shading. Following the observations made in this study, the most pronounced changes will occur on south aspects. This loss of canopy shading and the reduced albedo have been shown to increase the potential for mid-winter melt in middle snow zones of the California Sierra Nevada mountains (Hatchett et al., 2023). The results from the Sierra Nevada and my observations of alterations to the energy balance suggest that snow persistence would decrease in the low, early, and middle snow zones following wildfire. In the middle snow zone, snow persistence would decrease since early season

snowstorms since the likelihood of early season snow melting completely is greater without the shading from the canopy. I also predict spring melt to initiate earlier in the spring due to the increased radiative forcing from the lack of canopy and the decreased surface albedo. In the low and early season snow zones, snow persistence will decline due to complete melting occurring quicker after a storm due to the lack of shading not regulating the air temperature and radiative forcing which drive snow melt. Finally, the late season storms which were critical in dampening the albedo effects of the wildfire within the persistent snow zone occur less frequently at lower elevations (Figure 15b; McGrath et al., 2023), allowing the increased incoming shortwave energy to greatly alter the energy balance of the snowpack.

### **5.3.3 Influence of Snow Regime**

My study of wildfire effects in complex terrain adds to the rapidly growing body of site-specific studies that have occurred across the western U.S. in wildfire impacted areas (Koshkin et al., 2022). However, while many of the previous studies on wildfire and seasonal snow interactions focused on albedo and mass balance differences post-wildfire, most did not directly measure the differences in energy balance between burned and unburned sites. While albedo is a primary driver for snowmelt processes in all mid-latitude snow regimes (Painter, Molotch, et al., 2007), snowpack mechanics throughout the entire snow-on period can vary greatly based on snow regime (Trujillo & Molotch, 2014). The implications of varied snow regimes when considering both climate change and the impact of wildfire presents the need for nuanced understanding of energy and mass balances in each snow regime.

Many studies of wildfire-snow interactions have taken place in maritime snow climates (Gleason & Nolin, 2016; Koshkin et al., 2022; Uecker et al., 2020), however these studies did

not directly compare burned and unburned energy balances, so here I will focus on how energy balance dynamics in maritime regions may be altered from my findings in the continental snow regime. The maritime regime is defined by high quantities of SWE accumulating rapidly before precipitous melt occurs each spring. Due to the high variability and high potential for long durations of no new snow, the darkening of surface albedo can lead to significant mid-winter melt within wildfire burned areas as shown by Hatchett et al. (2023). In areas like the Pacific Northwest, longwave energy can be the dominant energy balance component, regulating the timing and rate of snow melt (Kraft et al., 2022). In these areas, the loss of longwave energy from the canopy might alter the snowpack similarly to what was observed in this study, where the lack of longwave energy resulted in greater cold content during the early portions of the accumulation season. However, the loss of this canopy during wildfire could then lead to significantly greater melt rates than pre-wildfire due to the dominant energy balance component changing from net longwave radiation to net shortwave. Additionally, following wildfire there would be an expected decrease in albedo which would become even more important in a shortwave-dominant regime.

## 6. FUTURE WORK

Given the increase in wildfire burned area and frequency within high-elevation areas and the persistent snow zone across the western U.S., coupled with the impacts of wildfire on snowpack energy and mass balances, hydrologic and ecological fluxes, and water quality and quantity additional plot- and large-scale research is required. Directly building off the aspect-based mass balance analysis presented in this thesis would be a study summarizing the aspect-based changes in energy balance between burned and unburned areas. By completing the energy balance portion of this work, direct relationships could be identified between observed energy fluxes and observed accumulation and melt patterns. Directly constraining the energy and mass balance relationships in wildfire impacted persistent snow zones, model parameterization could then be improved so future physical modelling of watershed could incorporate accurate energy balances for burned areas.

The immense data collection efforts conducted within the Cameron Peak burn area allows for analysis that is unique and exciting. Following the 2022–23 winter, there will be weekly to monthly snowpack measurements (snow pit and depth transects) within the Cameron Peak wildfire burn area for the three years following the disturbance. Using this in-situ data and hourly data from the automated weather stations and time-lapse cameras enables a project to evaluate the ways that snowpack processes have evolved over the three years since the fire. While some work has been completed on trying to understand the evolution of albedo impacts in the burned area (Gleason et al., 2019; Uecker et al., 2020), these projects have been limited by the need to use space-for-time study designs. The data available within the Cameron Peak fire eliminates the need for a space-for-time study and would allow for direct analysis of the evolution of snowpack processes for three years following the wildfire disturbance. Additionally, the changing

soot/debris deposition patterns would further allow this study to contribute to a better understanding of how important the deposition of soot/debris is to the energy cycle in compared to the increased incoming shortwave energy. In the modelling framework, the automated weather station point observations could be used to drive and evaluate the outputs from physical models like iSnobal and SnowModel which are very powerful but are not yet proven in a burned setting.

Further, comparing these multi-year data sets to other data sets collected locally and in other ecoregions could also be an important contribution and allow for a better understanding of how regional differences in snow zone and ecoregion might alter the impact and evolution of wildfire. While the persistent snow zone of the Cameron Peak wildfire area is currently instrumented to analyze differences between unburned and highly burned areas, it is also important to better constrain how burn severity gradients alter the impacts of wildfire. Supplementing the current study area to capture a wider range of burn conditions would be difficult due to the burned/unburned nature of the study area but working in other areas or adding sites within the burned zone of other wildfires would allow for further analysis. Also, expanding the analysis used in this study to capture low, early, middle, and late snow zones would reveal differences in how the energy balance is altered following wildfire across a variety of snow zones and elevations.

A major push in the snow and snow hydrology community currently is the application of remote sensing technologies to identify changes in SWE and surface albedo to help drive physical models (Meyer et al., 2023b; Molotch et al., 2004). Recent studies have shown the ability to identify snow surface albedo at subpixel scales within wildfire burned areas (Hatchett et al., 2023), which opens the door to new inquiries analyzing the evolution of snow surface albedo through the melt season and across multiple seasons in wildfire burn areas. Additionally,

this analysis of sub-pixel retrievals allows for a combination of in-situ and remote sensing to compare the albedo in areas with high and low mortality prior to the fire and tracking how the albedo evolves over seasonal to multi-year timescales. The expansion from local to regional scales will likely rely on previous plot scale studies to provide more nuanced analysis of how the local characteristics of ecosystems and wildfire impact watersheds and snowpacks differently across the western U.S.

## 7. CONCLUSIONS

Using season-long paired in-situ and automated weather station measurements, I investigated the mass and energy balance impacts following wildfire to a high-elevation seasonal snowpack in complex terrain. My research shows that complex terrain in post-wildfire burned areas can greatly modulate the impacts of the wildfire with south burned aspects showing the greatest alterations in peak SWE timing, melt rates, and snow disappearance date. This comparison indicated that south aspect burned areas reached SDD at least 11 days before south unburned aspects while burned north aspect SDD occurred 4 days earlier to similar unburned areas. I found no significant difference in peak SWE quantity between burned and unburned areas with similar aspects.

Through a comparison of the paired AWS data, I found that the net energy at the burned site had greater magnitudes over the entire winter season than the unburned site. During the beginning of the winter there was an increased energy deficit at the burned site due primarily to greater energy losses from both longwave radiation and the net turbulent balance. Following ~mid-April the increased net shortwave radiation at the burned site began to be the primary component of the energy balance. At the beginning of May the net energy at the burned site began to be greater than the energy balance at the unburned site. Through this work, I was able to quantify the compensating effects of wildfire in burned areas which have been hinted at in previous literature but never quantified. Within the burned area, I found that although there is less canopy interception, the effects of turbulent fluxes equate to negligible differences in peak SWE quantity. When focusing on the energy balance, the increased net shortwave energy into the snowpack from due to the lack of shading is offset by a decrease in the net longwave energy

through the winter until longer spring days and higher zenith angles begin to take over the energy balance, leading to little preconditioning of the seasonal snowpack.

Incorporating aspect-based analysis of SWE accumulation and melt following wildfire and paired energy balance analysis between burned and unburned areas furthers our understanding of how wildfire alters the physical processes within high-elevation seasonal snowpacks. This work will allow for better operational and scientific understanding of hydrology following wildfire in snow dominated watersheds, which is essential due to the importance of these snowpacks for downstream water users and the rapid increases in wildfire at these elevations since 2000 (Alizadeh et al., 2021; Iglesias et al., 2022; Kampf et al., 2022). By analyzing the alteration of the mass and energy balances following wildfire across complex terrain within a high-elevation continental snow zone, my research provides important analysis which can be used to improve modelling parameterizations, so water managers have the information they need to make inform decisions regarding water resource management following wildfire.

## REFERENCES

- Abatzoglou, J. T., Battisti, D. S., Williams, A. P., Hansen, W. D., Harvey, B. J., & Kolden, C. A. (2021). Projected increases in western US forest fire despite growing fuel constraints. *Communications Earth and Environment*, 2(1). <https://doi.org/10.1038/s43247-021-00299-0>
- Abatzoglou, J. T., & Williams, A. P. (2016). Impact of anthropogenic climate change on wildfire across western US forests. *Proceedings of the National Academy of Sciences of the United States of America*, 113(42), 11770–11775. <https://doi.org/10.1073/pnas.1607171113>
- Alizadeh, M. R., Abatzoglou, J. T., Luce, C. H., Adamowski, J. F., Farid, A., & Sadegh, M. (2021). Warming enabled upslope advance in western US forest fires. *Proceedings of the National Academy of Sciences of the United States of America*, 118(22). <https://doi.org/10.1073/pnas.2009717118>
- Anderson, B. T., McNamara, J. P., Marshall, H.-P., & Flores, A. N. (2014). Insights into the physical processes controlling correlations between snow distribution and terrain properties. *Water Resources Research*, 50(6), 4545–4563. <https://doi.org/10.1002/2013WR013714>
- Anderton, S. P., White, S. M., & Alvera, B. (2004). Evaluation of spatial variability in snow water equivalent for a high mountain catchment. *Process*, 18, 435–453. <https://doi.org/10.1002/hyp.1319>
- Andreas, E. L. (2002). *Parameterizing Scalar Transfer over Snow and Ice: A Review*.
- Bales, R. C., Molotch, N. P., Painter, T. H., Dettinger, M. D., Rice, R., & Dozier, J. (2006). Mountain hydrology of the western United States. *Water Resources Research*, 42(8). <https://doi.org/10.1029/2005WR004387>

- Barnett, T. P., Adam, J. C., & Lettenmaier, D. P. (2005). Potential impacts of a warming climate on water availability in snow-dominated regions. *Nature*, *438*(7066), 303–309.  
<https://doi.org/10.1038/nature04141>
- Barnhart, T. B., Molotch, N. P., Livneh, B., Harpold, A. A., Knowles, J. F., & Schneider, D. (2016). Snowmelt rate dictates streamflow. *Geophysical Research Letters*, *43*(15), 8006–8016. <https://doi.org/10.1002/2016GL069690>
- Biederman, J. A., Brooks, P. D., Harpold, A. A., Gochis, D. J., Gutmann, E., Reed, D. E., Pendall, E., & Ewers, B. E. (2014). Multiscale observations of snow accumulation and peak snowpack following widespread, insect-induced lodgepole pine mortality. *Ecohydrology*, *7*(1), 150–162. <https://doi.org/10.1002/eco.1342>
- Blankinship, J. C., Meadows, M. W., Lucas, R. G., & Hart, S. C. (2014). Snowmelt timing alters shallow but not deep soil moisture in the Sierra Nevada. *Water Resources Research*, *50*(2), 1448–1456. <https://doi.org/10.1002/2013WR014541>
- Bonnell, R., McGrath, D., Williams, K., Webb, R., Fassnacht, S. R., & Marshall, H. P. (2021). Spatiotemporal variations in liquid water content in a seasonal snowpack: Implications for radar remote sensing. *Remote Sensing*, *13*(21). <https://doi.org/10.3390/RS13214223>
- Boon, S. (2009). Snow ablation energy balance in a dead forest stand. *Hydrological Processes*, *23*(18), 2600–2610. <https://doi.org/10.1002/hyp.7246>
- Boon, S. (2012). Snow accumulation following forest disturbance. *Ecohydrology*, *5*(3), 279–285.  
<https://doi.org/10.1002/eco.212>
- Brutsaert, W. (1982). *Evaporation into the Atmosphere*. Springer Netherlands.  
<https://doi.org/10.1007/978-94-017-1497-6>

- Burles, K., & Boon, S. (2011). Snowmelt energy balance in a burned forest plot, Crowsnest Pass, Alberta, Canada. *Hydrological Processes*, 25(19), 3012–3029.  
<https://doi.org/10.1002/hyp.8067>
- Cameron Peak Fire BAER. (2020). <https://inciweb.nwcg.gov/incident/6964/>
- Cayan, D. R., Dettinger, M. D., Kammerdiener, S. A., Caprio, J. M., & Peterson, D. H. (2001). Changes in the Onset of Spring in the Western United States. *Bulletin of the American Meteorological Society*, 82(3), 399–415. [https://doi.org/10.1175/1520-0477\(2001\)082<0399:CITOOS>2.3.CO;2](https://doi.org/10.1175/1520-0477(2001)082<0399:CITOOS>2.3.CO;2)
- Clow, D. W. (2010). Changes in the timing of snowmelt and streamflow in Colorado: A response to recent warming. *Journal of Climate*, 23(9), 2293–2306.  
<https://doi.org/10.1175/2009JCLI2951.1>
- Clow, D. W., Williams, M. W., & Schuster, P. F. (2016). Increasing aeolian dust deposition to snowpacks in the Rocky Mountains inferred from snowpack, wet deposition, and aerosol chemistry. *Atmospheric Environment*, 146, 183–194.  
<https://doi.org/10.1016/j.atmosenv.2016.06.076>
- Cohen, J., Ye, H., & Jones, J. (2015). Trends and variability in rain-on-snow events. *Geophysical Research Letters*, 42(17), 7115–7122. <https://doi.org/10.1002/2015GL065320>
- Colorado River Basin Water Supply and Demand Study Executive Summary. (2012).
- Corriveau, J., Chambers, P. A., Yates, A. G., & Culp, J. M. (2011). Snowmelt and its role in the hydrologic and nutrient budgets of prairie streams. *Water Science and Technology*, 64(8), 1590–1596. <https://doi.org/10.2166/wst.2011.676>
- Davis, K. T., Robles, M. D., Kemp, K. B., Higuera, P. E., Chapman, T., Metlen, K. L., Peeler, J. L., Rodman, K. C., Woolley, T., Addington, R. N., Buma, B. J., Cansler, C. A., Case, M. J.,

- Collins, B. M., Coop, J. D., Dobrowski, S. Z., Gill, N. S., Haffey, C., Harris, L. B., ...  
Campbell, J. L. (2023). Reduced fire severity offers near-term buffer to climate-driven declines in conifer resilience across the western United States. *Proceedings of the National Academy of Sciences of the United States of America*, 120(11).  
<https://doi.org/10.1073/pnas.2208120120>
- Dennison, P. E., Brewer, S. C., Arnold, J. D., & Moritz, M. A. (2014). Large wildfire trends in the western United States, 1984-2011. *Geophysical Research Letters*, 41(8), 2928–2933.  
<https://doi.org/10.1002/2014GL059576>
- Dozier, J. (1980). A clear-sky spectral solar radiation model for snow-covered mountainous terrain. *Water Resources Research*, 16(4), 709–718.  
<https://doi.org/10.1029/WR016i004p00709>
- Dozier, J., Bair, E. H., & Davis, R. E. (2016a). Estimating the spatial distribution of snow water equivalent in the world's mountains. In *Wiley Interdisciplinary Reviews: Water* (Vol. 3, Issue 3, pp. 461–474). John Wiley and Sons Inc. <https://doi.org/10.1002/wat2.1140>
- Dozier, J., Bair, E. H., & Davis, R. E. (2016b). Estimating the spatial distribution of snow water equivalent in the world's mountains. *Wiley Interdisciplinary Reviews: Water*, 3(3), 461–474. <https://doi.org/10.1002/wat2.1140>
- Dudley, R. W., Hodgkins, G. A., McHale, M. R., Kolian, M. J., & Renard, B. (2017). Trends in snowmelt-related streamflow timing in the conterminous United States. *Journal of Hydrology*, 547, 208–221. <https://doi.org/10.1016/j.jhydrol.2017.01.051>
- Duguay, C. R. (1993). Radiation Modeling in Mountainous Terrain Review and Status. In *Source: Mountain Research and Development* (Vol. 13, Issue 4).  
<https://about.jstor.org/terms>

- Dye, D. G. (2002). Variability and trends in the annual snow-cover cycle in Northern Hemisphere land areas, 1972-2000. *Hydrological Processes*, 16(15), 3065–3077.  
<https://doi.org/10.1002/hyp.1089>
- Elder, K., Dozier, J., & Michaelsen, J. (1989). Spatial and Temporal Variation of Net Snow Accumulation in a Small Alpine Watershed, Emerald Lake Basin, Sierra Nevada, California, U.S.A. *Annals of Glaciology*, 13, 56–63.  
<https://doi.org/10.3189/s0260305500007643>
- Elder, K., Dozier, J., & Michaelsen, J. (1991). Snow accumulation and distribution in an Alpine Watershed. *Water Resources Research*, 27(7), 1541–1552.  
<https://doi.org/10.1029/91WR00506>
- Elder, K., Rosenthal, W., & Davis, R. E. (1998). Estimating the spatial distribution of snow water equivalence in a montane watershed. *Hydrological Processes*, 12(10–11).  
[https://doi.org/10.1002/\(SICI\)1099-1085\(199808/09\)12:10/11<1793::AID-HYP695>3.0.CO;2-K](https://doi.org/10.1002/(SICI)1099-1085(199808/09)12:10/11<1793::AID-HYP695>3.0.CO;2-K)
- Gersh, M., Gleason, K. E., & Surunis, A. (2022). Forest Fire Effects on Landscape Snow Albedo Recovery and Decay. *Remote Sensing*, 14(16). <https://doi.org/10.3390/rs14164079>
- Giovando, J., & Niemann, J. D. (2022). Wildfire Impacts on Snowpack Phenology in a Changing Climate Within the Western U.S. *Water Resources Research*, 58(8), e2021WR031569.  
<https://doi.org/10.1029/2021WR031569>
- Gleason, K. E., McConnell, J. R., Arienzo, M. M., Chellman, N., & Calvin, W. M. (2019). Four-fold increase in solar forcing on snow in western U.S. burned forests since 1999. *Nature Communications*, 10(1). <https://doi.org/10.1038/S41467-019-09935-Y>

- Gleason, K. E., McConnell, J. R., Arienzo, M. M., Sexstone, G. A., & Rahimi, S. (2022). Black carbon dominated dust in recent radiative forcing on Rocky Mountain snowpacks. *Environmental Research Letters*, *17*(5). <https://doi.org/10.1088/1748-9326/ac681b>
- Gleason, K. E., & Nolin, A. W. (2016). Charred forests accelerate snow albedo decay: parameterizing the post-fire radiative forcing on snow for three years following fire. *Hydrological Processes*, *30*(21), 3855–3870. <https://doi.org/10.1002/hyp.10897>
- Gleason, K. E., Nolin, A. W., & Roth, T. R. (2013). Charred forests increase snowmelt: Effects of burned woody debris and incoming solar radiation on snow ablation. *Geophysical Research Letters*, *40*(17), 4654–4661. <https://doi.org/10.1002/grl.50896>
- Granger, R. J., & Pomeroy, J. W. (1997). Sustainability of the western Canadian boreal forest under changing hydrological conditions. II. Summer energy and water use. *IAHS-AISH Publication*, *240*(December), 243–249.
- Groisman, P. Ya., Karl, T. R., & Knight, R. W. (1994). Observed Impact of Snow Cover on the Heat Balance and the Rise of Continental Spring Temperatures. *Science*, *263*(5144), 198–200. <https://doi.org/10.1126/science.263.5144.198>
- Hall, D. K., Crawford, C. J., DiGirolamo, N. E., Riggs, G. A., & Foster, J. L. (2015). Detection of earlier snowmelt in the wind river range, wyoming, using landsat imagery, 1972-2013. *Remote Sensing of Environment*, *162*, 45–54. <https://doi.org/10.1016/j.rse.2015.01.032>
- Hammond, J. C., & Kampf, S. K. (2020). Subannual Streamflow Responses to Rainfall and Snowmelt Inputs in Snow-Dominated Watersheds of the Western United States. *Water Resources Research*, *56*(4). <https://doi.org/10.1029/2019WR026132>

- Hammond, J. C., Saavedra, F. A., & Kampf, S. K. (2018). Global snow zone maps and trends in snow persistence 2001–2016. *International Journal of Climatology*, 38(12), 4369–4383. <https://doi.org/10.1002/joc.5674>
- Hammond, J. C., Sexstone, G. A., Putman, A. L., Barnhart, T. B., Rey, D. M., Driscoll, J. M., Liston, G. E., Rasmussen, K. L., McGrath, D., Fassnacht, S. R., & Kampf, S. K. (2023). High Resolution SnowModel Simulations Reveal Future Elevation-Dependent Snow Loss and Earlier, Flashier Surface Water Input for the Upper Colorado River Basin. *Earth's Future*, 11(2), e2022EF003092. <https://doi.org/10.1029/2022EF003092>
- Hardy, J. P., Davis, R. E., Jordan, R., Li, X., Woodcock, C., Ni, W., & McKenzie, J. C. (1997). Snow ablation modeling at the stand scale in a boreal jack pine forest. *Journal of Geophysical Research Atmospheres*, 102(24), 29397–29405. <https://doi.org/10.1029/96jd03096>
- Harpold, A. A., Biederman, J. A., Condon, K., Merino, M., Korgaonkar, Y., Nan, T., Sloat, L. L., Ross, M., & Brooks, P. D. (2014). Changes in snow accumulation and ablation following the Las Conchas Forest Fire, New Mexico, USA. *Ecohydrology*, 7(2), 440–452. <https://doi.org/10.1002/eco.1363>
- Hatchett, B. J., Koshkin, A. L., Guirguis, K., Rittger, K., Nolin, A. W., Heggli, A., Rhoades, A. M., East, A., Siirila-Woodburn, E. R., Brandt, W. T., Gershunov, A., & Haleakala, K. (2023). Midwinter dry spells amplify post-fire snowpack decline. *Geophysical Research Letters*. <https://doi.org/10.1029/2022GL101235>
- Hedstrom, N. R., & Pomeroy, J. W. (1998). Measurements and modelling of snow interception in the boreal forest. *Hydrological Processes*, 12(10–11), 1611–1625.

[https://doi.org/10.1002/\(SICI\)1099-1085\(199808/09\)12:10/11<1611::AID-HYP684>3.0.CO;2-4](https://doi.org/10.1002/(SICI)1099-1085(199808/09)12:10/11<1611::AID-HYP684>3.0.CO;2-4)

Iglesias, V., Balch, J. K., & Travis, W. R. (2022). U.S. fires became larger, more frequent, and more widespread in the 2000s. In *Sci. Adv* (Vol. 8, Issue 0020). <https://www.science.org>

Kampf, S. K., Mcgrath, D., Sears, M. G., Fassnacht, S. R., Kiewiet, L., & Hammond, J. C. (2022). *Increasing wildfire impacts on snowpack in the western U.S.*

<https://doi.org/10.1073/pnas>

Keller, F., Goyette, S., & Beniston, M. (2005). Sensitivity analysis of snow cover to climate change scenarios and their impact on plant habitats in alpine terrain. *Climatic Change*, 72(3), 299–319. <https://doi.org/10.1007/s10584-005-5360-2>

Klos, P. Z., Link, T. E., & Abatzoglou, J. T. (2014). Extent of the rain-snow transition zone in the western U.S. under historic and projected climate. *Geophysical Research Letters*, 41(13), 4560–4568. <https://doi.org/10.1002/2014GL060500>

Koshkin, A. L., Hatchett, B. J., & Nolin, A. W. (2022). Wildfire impacts on western United States snowpacks. *Frontiers in Water*, 0, 138. <https://doi.org/10.3389/FRWA.2022.971271>

Kraft, M., McNamara, J. P., Marshall, H.-P., & Glenn, N. F. (2022). Forest impacts on snow accumulation and melt in a semi-arid mountain environment. *Frontiers in Water*, 4. <https://doi.org/10.3389/frwa.2022.1004123>

Lee, W. L., Liou, K. N., & Hall, A. (2011). Parameterization of solar fluxes over mountain surfaces for application to climate models. *Journal of Geophysical Research Atmospheres*, 116(1). <https://doi.org/10.1029/2010JD014722>

- Li, D., Wrzesien, M. L., Durand, M., Adam, J., & Lettenmaier, D. P. (2017). How much runoff originates as snow in the western United States, and how will that change in the future? *Geophysical Research Letters*, *44*(12), 6163–6172. <https://doi.org/10.1002/2017GL073551>
- Li, J., Okin, G. S., McKenzie Skiles, S., & Painter, T. H. (2013). Relating variation of dust on snow to bare soil dynamics in the western United States. *Environmental Research Letters*, *8*(4). <https://doi.org/10.1088/1748-9326/8/4/044054>
- Liston, G. E., Haehnel, R. B., Sturm, M., Hiemstra, C. A., Berezovskaya, S., & Tabler, R. D. (2007). Simulating complex snow distributions in windy environments using SnowTran-3D. *Journal of Glaciology*, *53*(181), 241–256. <https://doi.org/10.3189/172756507782202865>
- Livneh, B., & Badger, A. M. (2020). Drought less predictable under declining future snowpack. *Nature Climate Change*, *10*(5), 452–458. <https://doi.org/10.1038/s41558-020-0754-8>
- Loiselle, D., Du, X., Alessi, D. S., Bladon, K. D., & Faramarzi, M. (2020). Projecting impacts of wildfire and climate change on streamflow, sediment, and organic carbon yields in a forested watershed. *Journal of Hydrology*, *590*, 125403. <https://doi.org/10.1016/j.jhydrol.2020.125403>
- López-Moreno, J. I., Fassnacht, S. R., Beguería, S., & Latron, J. B. P. (2011). Variability of snow depth at the plot scale: Implications for mean depth estimation and sampling strategies. *Cryosphere*, *5*(3), 617–629. <https://doi.org/10.5194/tc-5-617-2011>
- Maina, F. Z., & Siirila-Woodburn, E. R. (2020). Watersheds dynamics following wildfires: Nonlinear feedbacks and implications on hydrologic responses. *Hydrological Processes*, *34*(1), 33–50. <https://doi.org/10.1002/hyp.13568>
- Mandal, A., Angchuk, T., Azam, M. F., Ramanathan, A., Wagnon, P., Soheb, M., & Singh, C. (2022). An 11-year record of wintertime snow-surface energy balance and sublimation at

- 4863ma.s.l. on the Chhota Shigri Glacier moraine (western Himalaya, India). *Cryosphere*, 16(9), 3775–3799. <https://doi.org/10.5194/tc-16-3775-2022>
- Marks, D., & Dozier, J. (1992). Climate and energy exchange at the snow surface in the Alpine Region of the Sierra Nevada: 2. Snow cover energy balance. *Water Resources Research*, 28(11), 3043–3054. <https://doi.org/10.1029/92WR01483>
- Marks, D., Dozier, J., & Davis, R. E. (1992). Climate and energy exchange at the snow surface in the Alpine Region of the Sierra Nevada: 1. Meteorological measurements and monitoring. *Water Resources Research*, 28(11), 3029–3042. <https://doi.org/10.1029/92WR01482>
- Marshall, A. M., Abatzoglou, J. T., Link, T. E., & Tennant, C. J. (2019). Projected Changes in Interannual Variability of Peak Snowpack Amount and Timing in the Western United States. *Geophysical Research Letters*, 46(15), 8882–8892. <https://doi.org/10.1029/2019GL083770>
- Marshall, H. P., Vuyovich, C., Hiemstra, C., Brucker, L., Elder, K., Deems, J., & Newlin, J. (2019). *NASA SnowEx 2020 Experiment Plan (Science Plan)*.
- Mathys, A. S., Coops, N. C., & Waring, R. H. (2017). An ecoregion assessment of projected tree species vulnerabilities in western North America through the 21st century. *Global Change Biology*, 23(2), 920–932. <https://doi.org/10.1111/gcb.13440>
- Maxwell, J. D., Call, A., & St. Clair, S. B. (2019). Wildfire and topography impacts on snow accumulation and retention in montane forests. *Forest Ecology and Management*, 432(May 2018), 256–263. <https://doi.org/10.1016/j.foreco.2018.09.021>

- McCabe, G. J., & Clark, M. P. (2005). Trends and Variability in Snowmelt Runoff in the Western United States. *Journal of Hydrometeorology*, 6(4), 476–482.  
<https://doi.org/10.1175/JHM428.1>
- McCabe, G. J., Clark, M. P., & Hay, L. E. (2007). Rain-on-Snow Events in the Western United States. *Bulletin of the American Meteorological Society*, 88(3), 319–328.  
<https://doi.org/10.1175/BAMS-88-3-319>
- McGrath, D., Zeller, L., Bonnell, R., Reis, W., Kampf, S., Williams, K., Okal, M., Olsen-Mikitowicz, A., Bump, E., Sears, M., & Rittger, K. (2023). Declines in Peak Snow Water Equivalent and Elevated Snowmelt Rates Following the 2020 Cameron Peak Wildfire in Northern Colorado. *Geophysical Research Letters*, 50(6).  
<https://doi.org/10.1029/2022GL101294>
- Meyer, J., Horel, J., Kormos, P., Hedrick, A., Trujillo, E., & Skiles, S. M. (2023a). Operational water forecast ability of the HRRR-iSnobal combination: an evaluation to adapt into production environments. *Geoscientific Model Development*, 16(1), 233–250.  
<https://doi.org/10.5194/gmd-16-233-2023>
- Meyer, J., Horel, J., Kormos, P., Hedrick, A., Trujillo, E., & Skiles, S. M. (2023b). Operational water forecast ability of the HRRR-iSnobal combination: an evaluation to adapt into production environments. *Geoscientific Model Development*, 16(1), 233–250.  
<https://doi.org/10.5194/gmd-16-233-2023>
- Michalsky, J. J., & Hodges, G. B. (2013). Field measured spectral albedo-four years of data from the western u.s. Prairie. *Journal of Geophysical Research Atmospheres*, 118(2), 813–825.  
<https://doi.org/10.1002/jgrd.50149>

- Miller, Z. S., Peitzsch, E. H., Sproles, E. A., Birkeland, K. W., & Palomaki, R. T. (2022). Assessing the seasonal evolution of snow depth spatial variability and scaling in complex mountain terrain. *The Cryosphere*, *16*(12), 4907–4930. <https://doi.org/10.5194/tc-16-4907-2022>
- Moeser, C. D., Broxton, P. D., Harpold, A., & Robertson, A. (2020). Estimating the Effects of Forest Structure Changes From Wildfire on Snow Water Resources Under Varying Meteorological Conditions. *Water Resources Research*, *56*(11), 1–23. <https://doi.org/10.1029/2020WR027071>
- Molotch, N. P., & Bales, R. C. (2006). SNOTEL representativeness in the Rio Grande headwaters on the basis of physiographics and remotely sensed snow cover persistence. *Hydrological Processes*, *20*(4), 723–739. <https://doi.org/10.1002/hyp.6128>
- Molotch, N. P., Blanken, P. D., Williams, M. W., Turnipseed, A. A., Monson, R. K., & Margulis, S. A. (2007). Estimating sublimation of intercepted and sub-canopy snow using eddy covariance systems. *Hydrological Processes*, *21*(12), 1567–1575. <https://doi.org/10.1002/hyp.6719>
- Molotch, N. P., Brooks, P. D., Burns, S. P., Litvak, M., Monson, R. K., McConnell, J. R., & Musselman, K. (2009). Ecohydrological controls on snowmelt partitioning in mixed-conifer sub-alpine forests. *Ecohydrology*, *2*(2), 129–142. <https://doi.org/10.1002/eco.48>
- Molotch, N. P., Colee, M. T., Bales, R. C., & Dozier, J. (2005). Estimating the spatial distribution of snow water equivalent in an alpine basin using binary regression tree models: The impact of digital elevation data and independent variable selection. *Hydrological Processes*, *19*(7), 1459–1479. <https://doi.org/10.1002/hyp.5586>

- Molotch, N. P., Painter, T. H., Bales, R. C., & Dozier, J. (2004). Incorporating remotely-sensed snow albedo into a spatially-distributed snowmelt model. *Geophysical Research Letters*, *31*(3), 1–4. <https://doi.org/10.1029/2003GL019063>
- Montesi, J., Elder, K., Schmidt, R. A., & Davis, R. E. (2004). Sublimation of Intercepted Snow within a Subalpine Forest Canopy at Two Elevations. *Journal of Hydrometeorology*, *5*(5), 763–773. [https://doi.org/10.1175/1525-7541\(2004\)005<0763:SOISWA>2.0.CO;2](https://doi.org/10.1175/1525-7541(2004)005<0763:SOISWA>2.0.CO;2)
- Moore, C., Kampf, S., Stone, B., & Richer, E. (2015). A GIS-based method for defining snow zones: application to the western United States. *Geocarto International*, *30*(1), 62–81. <https://doi.org/10.1080/10106049.2014.885089>
- Mote, P. W. (2006). *Climate-Driven Variability and Trends in Mountain Snowpack in Western North America\**. [www.wcc.nrcs](http://www.wcc.nrcs).
- Mote, P. W., Hamlet, A. F., Clark, M. P., & Lettenmaier, D. P. (2005). DECLINING MOUNTAIN SNOWPACK IN WESTERN NORTH AMERICA\*. *Bulletin of the American Meteorological Society*, *86*(1), 39–50. <https://doi.org/10.1175/BAMS-86-1-39>
- Mote, P. W., Li, S., Lettenmaier, D. P., Xiao, M., & Engel, R. (2018). Dramatic declines in snowpack in the western US. *Npj Climate and Atmospheric Science*, *1*(1), 2. <https://doi.org/10.1038/s41612-018-0012-1>
- Mott, R., Scipi3n, D., Schneebeli, M., Dawes, N., Berne, A., & Lehning, M. (2014). Orographic effects on snow deposition patterns in mountainous terrain. *Journal of Geophysical Research*, *119*(3), 1419–1439. <https://doi.org/10.1002/2013JD019880>
- Mueller, S. E., Thode, A. E., Margolis, E. Q., Yocom, L. L., Young, J. D., & Iniguez, J. M. (2020). Climate relationships with increasing wildfire in the southwestern US from 1984 to

2015. *Forest Ecology and Management*, 460.  
<https://doi.org/10.1016/J.FORECO.2019.117861>
- Murray, C. D., & Buttle, J. M. (2003). Impacts of clearcut harvesting on snow accumulation and melt in a northern hardwood forest. *Journal of Hydrology*, 271(1–4), 197–212.  
[https://doi.org/10.1016/S0022-1694\(02\)000352-9](https://doi.org/10.1016/S0022-1694(02)000352-9)
- Murray, F. W. (1967). On the Computation of Saturation Vapor Pressure. *Journal of Applied Meteorology*, 6(1), 203–204. [https://doi.org/10.1175/1520-0450\(1967\)006<0203:OTCOSV>2.0.CO;2](https://doi.org/10.1175/1520-0450(1967)006<0203:OTCOSV>2.0.CO;2)
- Musselman, K. N., Clark, M. P., Liu, C., Ikeda, K., & Rasmussen, R. (2017). Slower snowmelt in a warmer world. *Nature Climate Change*, 7(3), 214–219.  
<https://doi.org/10.1038/nclimate3225>
- Musselman, K. N., Molotch, N. P., & Brooks, P. D. (2008). Effects of vegetation on snow accumulation and ablation in a mid-latitude sub-alpine forest. *Hydrological Processes*, 22(15), 2767–2776. <https://doi.org/10.1002/HYP.7050>
- Namias, J. (1985). Some Empirical Evidence for the Influence of Snow Cover on Temperature and Precipitation. *Monthly Weather Review*, 113(9), 1542–1553.  
[https://doi.org/10.1175/1520-0493\(1985\)113<1542:SEEFTI>2.0.CO;2](https://doi.org/10.1175/1520-0493(1985)113<1542:SEEFTI>2.0.CO;2)
- O’Leary, D. S., Bloom, T. D., Smith, J. C., Zemp, C. R., & Medler, M. J. (2016). A new method comparing snowmelt timing with annual area burned. *Fire Ecology*, 12(1), 41–51.  
<https://doi.org/10.4996/fireecology.1201041>
- O’Leary III, D., Hall, D. K., Medler, M., Matthews, R., & Flower, A. (2019). *Snowmelt Timing Maps Derived from MODIS for North America, Version 2, 2001-2018*. ORNL DAAC.

- Painter, T. H., Barrett, A. P., Landry, C. C., Neff, J. C., Cassidy, M. P., Lawrence, C. R., McBride, K. E., & Farmer, G. L. (2007). Impact of disturbed desert soils on duration of mountain snow cover. *Geophysical Research Letters*, *34*(12), 1–6.  
<https://doi.org/10.1029/2007GL030284>
- Painter, T. H., Molotch, N. P., Cassidy, M., Flanner, M., & Steffen, K. (2007). Contact spectroscopy for determination of stratigraphy of snow optical grain size. *Journal of Glaciology*, *53*(180), 121–127. <https://doi.org/10.3189/172756507781833947>
- Picard, G., Dumont, M., Lamare, M., Tuzet, F., Larue, F., Pirazzini, R., & Arnaud, L. (2020). Spectral albedo measurements over snow-covered slopes: Theory and slope effect corrections. *Cryosphere*, *14*(5), 1497–1517. <https://doi.org/10.5194/tc-14-1497-2020>
- Pomeroy, J. W., Gray, D. M., Shook, K. R., Toth, B., Essery, R. L. H., Pietroniro, A., & Hedstrom, N. (1998). An evaluation of snow accumulation and ablation processes for land surface modelling. *Hydrological Processes*, *12*(15), 2339–2367.  
[https://doi.org/10.1002/\(SICI\)1099-1085\(199812\)12:15<2339::AID-HYP800>3.0.CO;2-L](https://doi.org/10.1002/(SICI)1099-1085(199812)12:15<2339::AID-HYP800>3.0.CO;2-L)
- Rodman, K. C., Veblen, T. T., Battaglia, M. A., Chambers, M. E., Fornwalt, P. J., Holden, Z. A., Kolb, T. E., Ouzts, J. R., & Rother, M. T. (2020). A changing climate is snuffing out post-fire recovery in montane forests. *Global Ecology and Biogeography*, *29*(11), 2039–2051.  
<https://doi.org/10.1111/geb.13174>
- Rodman, K. C., Veblen, T. T., Chapman, T. B., Rother, M. T., Wion, A. P., & Redmond, M. D. (2020). Limitations to recovery following wildfire in dry forests of southern Colorado and northern New Mexico, USA. *Ecological Applications*, *30*(1).  
<https://doi.org/10.1002/eap.2001>

- Roth, T. R., & Nolin, A. W. (2017). Forest impacts on snow accumulation and ablation across an elevation gradient in a temperate montane environment. *Hydrology and Earth System Sciences*, 21(11), 5427–5442. <https://doi.org/10.5194/HESS-21-5427-2017>
- Rother, M. T., & Veblen, T. T. (2016). Limited conifer regeneration following wildfires in dry ponderosa pine forests of the Colorado Front Range. *Ecosphere*, 7(12). <https://doi.org/10.1002/ecs2.1594>
- Schneider, D., & Molotch, N. P. (2016). Real-time estimation of snow water equivalent in the Upper Colorado River Basin using MODIS-based SWE Reconstructions and SNOTEL data. *Water Resources Research*, 52(10), 7892–7910. <https://doi.org/10.1002/2016WR019067>
- Seidl, R., Thom, D., Kautz, M., Martin-Benito, D., Peltoniemi, M., Vacchiano, G., Wild, J., Ascoli, D., Petr, M., Honkaniemi, J., Lexer, M. J., Trotsiuk, V., Mairota, P., Svoboda, M., Fabrika, M., Nagel, T. A., & Reyer, C. P. O. (2017). Forest disturbances under climate change. In *Nature Climate Change* (Vol. 7, Issue 6, pp. 395–402). Nature Publishing Group. <https://doi.org/10.1038/nclimate3303>
- Serreze, M. C., Clark, M. P., Armstrong, R. L., McGinnis, D. A., & Pulwarty, R. S. (1999). Characteristics of the western United States snowpack from snowpack telemetry (SNOTEL) data. *Water Resources Research*, 35(7), 2145–2160. <https://doi.org/10.1029/1999WR900090>
- Sexstone, G. A., Clow, D. W., Fassnacht, S. R., Liston, G. E., Hiemstra, C. A., Knowles, J. F., & Penn, C. A. (2018). Snow Sublimation in Mountain Environments and Its Sensitivity to Forest Disturbance and Climate Warming. *Water Resources Research*, 54(2), 1191–1211. <https://doi.org/10.1002/2017WR021172>

- Sexstone, G. A., Penn, C. A., Liston, G. E., Gleason, K. E., Moeser, C. D., & Clow, D. W. (2020). Spatial Variability in Seasonal Snowpack Trends across the Rio Grande Headwaters (1984–2017). *Journal of Hydrometeorology*, 21(11), 2713–2733. <https://doi.org/10.1175/JHM-D-20-0077.1>
- Shi, K., & Touge, Y. (2023). Identifying the shift in global wildfire weather conditions over the past four decades: an analysis based on change-points and long-term trends. 10, 3. <https://doi.org/10.1186/s40562-022-00255-6>
- Sicart, J. E., Pomeroy, J. W., Essery, R. L. H., & Bewley, D. (2006). Incoming longwave radiation to melting snow: Observations, sensitivity and estimation in northern environments. *Hydrological Processes*, 20(17), 3697–3708. <https://doi.org/10.1002/hyp.6383>
- Siirila-Woodburn, E. R., Rhoades, A. M., Hatchett, B. J., Huning, L. S., Szinai, J., Tague, C., Nico, P. S., Feldman, D. R., Jones, A. D., Collins, W. D., & Kaatz, L. (2021). A low-to-no snow future and its impacts on water resources in the western United States. *Nature Reviews Earth & Environment*, 2(11), 800–819. <https://doi.org/10.1038/s43017-021-00219-y>
- Sirguey, P., Mathieu, R., & Arnaud, Y. (2009). Subpixel monitoring of the seasonal snow cover with MODIS at 250 m spatial resolution in the Southern Alps of New Zealand: Methodology and accuracy assessment. *Remote Sensing of Environment*, 113(1), 160–181. <https://doi.org/10.1016/j.rse.2008.09.008>
- Skiles, S. M. K., Flanner, M., Cook, J. M., Dumont, M., & Painter, T. H. (2018). Radiative forcing by light-absorbing particles in snow. In *Nature Climate Change* (Vol. 8, Issue 11, pp. 964–971). Nature Publishing Group. <https://doi.org/10.1038/s41558-018-0296-5>

- Smoot, E. E., & Gleason, K. E. (2021). Forest Fires Reduce Snow-Water Storage and Advance the Timing of Snowmelt across the Western U.S. *Water*, 13(24), 3533.  
<https://doi.org/10.3390/w13243533>
- Stanke, H., Finley, A. O., Domke, G. M., Weed, A. S., & MacFarlane, D. W. (2021). Over half of western United States' most abundant tree species in decline. *Nature Communications*, 12(1). <https://doi.org/10.1038/s41467-020-20678-z>
- Stevens-Rumann, C. S., Kemp, K. B., Higuera, P. E., Harvey, B. J., Rother, M. T., Donato, D. C., Morgan, P., & Veblen, T. T. (2018). Evidence for declining forest resilience to wildfires under climate change. In *Ecology Letters* (Vol. 21, Issue 2, pp. 243–252). Blackwell Publishing Ltd. <https://doi.org/10.1111/ele.12889>
- Stevens-Rumann, C. S., & Morgan, P. (2019). Tree regeneration following wildfires in the western US: a review. In *Fire Ecology* (Vol. 15, Issue 1). SpringerOpen.  
<https://doi.org/10.1186/s42408-019-0032-1>
- Storck, P., Lettenmaier, D. P., & Bolton, S. M. (2002). Measurement of snow interception and canopy effects on snow accumulation and melt in a mountainous maritime climate, Oregon, United States. *Water Resources Research*, 38(11), 5-1-5–16.  
<https://doi.org/10.1029/2002wr001281>
- Sturm, M., Goldstein, M. A., & Parr, C. (2017). Water and life from snow: A trillion dollar science question. *Water Resources Research*, 53(5), 3534–3544.  
<https://doi.org/10.1002/2017WR020840>
- Sturm, M., Holmgren, J., & Liston, G. E. (1995). A Seasonal Snow Cover Classification System for Local to Global Applications. *Journal of Climate*, 8(5), 1261–1283.  
[https://doi.org/10.1175/1520-0442\(1995\)008<1261:ASSCCS>2.0.CO;2](https://doi.org/10.1175/1520-0442(1995)008<1261:ASSCCS>2.0.CO;2)

- Sturm, M., & Liston, G. E. (2021). Revisiting the Global Seasonal Snow Classification: An Updated Dataset for Earth System Applications. *Journal of Hydrometeorology*, 22(11), 2917–2938. <https://doi.org/10.1175/JHM-D-21-0070.1>
- Troendle, C. A., & King, R. M. (1985). The Effect of Timber Harvest on the Fool Creek Watershed, 30 Years Later. *Water Resources Research*, 21(12), 1915–1922. <https://doi.org/10.1029/WR021i012p01915>
- Trujillo, E., & Molotch, N. P. (2014). Snowpack regimes of the Western United States. *Water Resources Research*, 50(7), 5611–5623. <https://doi.org/10.1002/2013WR014753>
- Trujillo, E., Ramírez, J. A., & Elder, K. J. (2007). Topographic, meteorologic, and canopy controls on the scaling characteristics of the spatial distribution of snow depth fields. *Water Resources Research*, 43(7). <https://doi.org/10.1029/2006WR005317>
- Trujillo, E., Ramírez, J. A., & Elder, K. J. (2009). Scaling properties and spatial organization of snow depth fields in sub-alpine forest and alpine tundra. *Hydrological Processes*, 23(11), 1575–1590. <https://doi.org/10.1002/hyp.7270>
- Uecker, T. M., Kaspari, S. D., Musselman, K. N., & Skiles, S. M. (2020). The post-wildfire impact of burn severity and age on black carbon snow deposition and implications for snow water resources, cascade range, Washington. *Journal of Hydrometeorology*, 21(8), 1777–1792. <https://doi.org/10.1175/JHM-D-20-0010.1>
- Viviroli, D., Dürr, H. H., Messerli, B., Meybeck, M., & Weingartner, R. (2007). Mountains of the world, water towers for humanity: Typology, mapping, and global significance. *Water Resources Research*, 43(7). <https://doi.org/10.1029/2006WR005653>

- Wagner, A. M., Bennett, K. E., Liston, G. E., Hiemstra, C. A., & Cooley, D. (2021). Multiple indicators of extreme changes in snow-dominated streamflow regimes, Yakima river basin region, USA. *Water (Switzerland)*, *13*(19). <https://doi.org/10.3390/w13192608>
- Webb, R., Litvak, M., & Brooks, P. D. (2023). The role of terrain-mediated hydroclimate in vegetation recovery after wildfire. *Environmental Research Letters*.  
<https://doi.org/10.1088/1748-9326/acd803>
- Westerling, A. L. (2016). Increasing western US forest wildfire activity: sensitivity to changes in the timing of spring. *Philosophical Transactions of the Royal Society B: Biological Sciences*, *371*(1696), 20150178. <https://doi.org/10.1098/rstb.2015.0178>
- Westerling, A. L., Hidalgo, H. G., Cayan, D. R., & Swetnam, T. W. (2006). Warming and Earlier Spring Increase Western U.S. Forest Wildfire Activity. *Science*, *313*(5789), 940–943.  
<https://doi.org/10.1126/science.1128834>
- Westerling, A. L., Turner, M. G., Smithwick, E. A. H., Romme, W. H., & Ryan, M. G. (2011). Continued warming could transform greater yellowstone fire regimes by mid-21st century. *Proceedings of the National Academy of Sciences of the United States of America*, *108*(32), 13165–13170. <https://doi.org/10.1073/pnas.1110199108>
- Williams, L. D., Barry, R. G., & Andrews, J. T. (1972). Application of computed global radiation for areas of high relief. *Journal of Applied Meteorology*, *11*, 526–533.  
<https://doi.org/10.1175/1520-04501972011<0526:aocgrf<2.0.co;2>
- Winkler, R. D., Spittlehouse, D. L., & Golding, D. L. (2005). Measured differences in snow accumulation and melt among clearcut, juvenile, and mature forests in southern British Columbia. *Hydrological Processes*, *19*(1), 51–62. <https://doi.org/10.1002/hyp.5757>

Wrzesien, M. L., Durand, M. T., Pavelsky, T. M., Kapnick, S. B., Zhang, Y., Guo, J., & Shum,

C. K. (2018). A New Estimate of North American Mountain Snow Accumulation From Regional Climate Model Simulations. *Geophysical Research Letters*, *45*(3), 1423–1432.

<https://doi.org/10.1002/2017GL076664>

Zhang, T. (2005). Influence of the seasonal snow cover on the ground thermal regime: An overview. In *Reviews of Geophysics* (Vol. 43, Issue 4).

<https://doi.org/10.1029/2004RG000157>